The CD36 scavenger receptor Bez regulates lipid redistribution from fat body to oocytes in Drosophila

Pilar Carrera[1], Johanna Odenthal[2], Katharina S. Risse[1], Yerin Jung[1], Lars Kuerschner[1], Margret H. Bülow[1#]

1 Life and Medical Sciences (LIMES), University of Bonn, Carl-Troll-Straße 31, 53115 Bonn, Germany
2 Department II of Internal Medicine and Center for Molecular Medicine Cologne, Faculty of Medicine, University of Cologne, University Hospital Cologne, Cologne, Germany

correspondence to: mbuelow@uni-bonn.de

Abstract

Class B scavenger receptors of the CD36 family are important for lipid mobilization from mammalian adipose tissue. This protein family has 3 members in mammals, but 14 in *Drosophila melanogaster*. Lipid distribution in *Drosophila* is mediated by homologs of the LDL receptors, while little is known about the function of scavenger receptors for this process in invertebrates. Here we unravel a role for the so far uncharacterized scavenger receptor Bez in lipid export from *Drosophila* adipocytes. Bez shares the lipid binding residue with CD36 and is expressed at the plasma membrane of the embryonic, larval and adult fat body. Bez loss-of-function lowers the organismal content of storage lipids while they accumulate in the fat body, concomitant with female sterility and degeneration of ovaries. Using an alkyne-labeled fatty acid tracer, we demonstrate that Bez interacts with the apoB homolog Lipophorin at the plasma membrane of adipocytes, thereby enabling lipid transfer. Our study shows how a scavenger receptor interacts with lipoproteins to distribute storage lipids from the fat body to the ovaries and thereby contributes to the metabolic control of development.

Introduction

Scavenger receptors (SR) are a family of transmembrane proteins that are structurally diverse and have a wide range of ligands. They were first discovered in macrophages as receptors for oxidized Low Density Lipoprotein (oxLDL) (Goldstein et al., 1979; Brown et al., 1980). Further studies showed that SR act as multifunctional receptors implicated in a range of cellular processes. Apart from modified lipoproteins like oxLDL, many other endogenous, mainly polyanionic ligands have been identified, such as long chain fatty acids, oxidized phospholipids and extracellular matrix proteins (Rigotti et al., 1995; Silverstein and Febbraio 2009). SR can be sorted in eight different classes depending on their predicted structure, which is determined by the presence of different conserved motifs (Krieger 1997; Plüddemann et al., 2007). Class B scavenger receptors (SR-B) are characterized by a hairpin structure, formed by two transmembrane domains and one extracellular loop with multiple glycosylation sites. The extracellular CD36-domain includes numerous ligand-binding sites (Canton et al., 2013) and its sequence is highly conserved between the different members of this SR

class. Its tertiary structure is defined by disulfide bonds between conserved cysteine residues, which are essential for the recognition of ligands (Gruarin et al., 1997). By contrast, the sequences of the relatively short, intracellular N- and C-terminal tails are not conserved. These tails interact with cytosolic proteins and regulate cellular signalling. SR-B can bind to a wide range of ligands, such as lipoproteins, long chain fatty acids and oxidized phospholipids. In contrast to the other SR classes, they are also able to bind to native lipoproteins such as LDL and HDL (high density lipoprotein) and thereby contribute to the regulation of lipid metabolism. Vertebrate SR-Bs comprise the proteins Cluster of Differentiation 36 (CD36), Scavenger receptor class B member I (SRBI) and Lysosomal integral membrane protein II (LIMP-II). CD36 and SRBI are located at the plasma membrane while LIMP-II is a protein of the lysosomal membrane with a function in the import of glucocerebrosidase (Heybrock et al., 2019).

CD36 is a multifunctional protein that regulates the uptake and export of fatty acids in gut cells, adipocytes and muscle cells (Daquinag et al., 2021). It is also expressed in taste bud cells where it acts as a lipid sensor for the detection of dietary lipids (Laugerette, 2005). Fatty acid transfer from adipocytes to ovarian tumours has been shown to depend on the CD36-dependent lipid uptake by adipocytes (Ladanyi et al., 2018). CD36 is also required for ovarian angiogenesis and folliculogenesis: CD36-deficient mice display hypervascularized ovaries and have less offspring than controls (Osz et al., 2014). However, this function has been linked to binding of thrombospondin-1, an angiogenesis regulator, and not to the lipid binding property of CD36.

In the invertebrate *Drosophila melanogaster*, 14 SR-B homologues have been identified (Nichols & Vogt, 2008). The high number of SR genes suggests a diversification of functions in insects. Many of these genes remain uncharacterized until now, but some have been functionally analysed. Croquemort (Crq) is expressed in macrophages and takes part in the phagocytosis of apoptotic cells during embryogenesis and the morphogenesis of the central nervous system (Guillou et al., 2016). Debris buster (Dsb) is a protein of the lysosomal membrane that is required for trafficking of extracellular matrix components important for airway physiology and for clearing of degenerating dendrites (Han et al., 2014; Wingen et al., 2017). Neither inactivation nor afterpotential-D (NinaD) and Scavenger receptor acting in neural tissue and majority of rhodopsin absent (Santa-Maria) were identified as transporters for carotenoids, precursors for the synthesis of vitamin A, which itself is modified and then embedded in the optical pigment Rhodopsin. NinaD is expressed in the gut where it mediates the uptake of carotenoids, which are required for visual chromophore synthesis. Santa-Maria is expressed in specific neurons and glia cells and locates to the plasma membrane, where it mediates the uptake of β-carotene that afterwards is converted to vitamin A (Dewett et al., 2021). Sensory neuron membrane protein 1 (SNMP1) is expressed in olfactory neurons and in steroidogenic organs such as the ovaries, testes and the prothoracic gland (PG). Silencing of SNMP1 via RNAi expression in the PG and in the follicle cells of the ovary results in a reduced content of lipid droplets in these tissues (Talamillo et al., 2013).

Lipid shuttling in both human blood and Drosophila hemolymph is mediated by lipoproteins. In Drosophila, apoLpp (Lipophorin) and apoLTP (Lipid transfer protein) belong to the apoB family of lipoproteins. The product of the *apoLpp* gene (CG11064) gives rise to apoLI and apoLII that assemble the Lipophorin lipoprotein. Human apoB is the major lipoprotein in LDL particles. Lpp binds to LTP in the gut and is loaded with dietary lipids. These are distributed to the fat body for storage and to other organs (Palm et al., 2012). The Drosophila fat body stores lipids in lipid droplets from where they are mobilized, e.g. upon starvation, to nurse other tissues. Fasting induces a morphological change of fat body lipid droplets as they become larger and fewer when lipids are mobilized (Ugrankar et al., 2019).

88 Nutrition is closely linked to reproduction. Malnutrition in women heavily impacts reproduction,
89 with both obesity and undernutrition affecting fertility (Silvestris et al., 2019). Also in *Drosophila*, this
90 link exists and Drosophila females store high amounts of triglycerides (TG), a neutral lipid known as
91 fat to support oocyte maturation. Uptake of neutral lipids takes place between stage 8 and 10 of
92 oocyte maturation: at stage 10, oocytes massively accumulate neutral lipids in both nurse cells and
93 follicle cells. Lipoproteins mediate the transfer of lipids from the hemolymph to ovaries (Sieber &
94 Spradling, 2015). In ovaries, lipophorin receptors bind LTP, which is required for neutral lipid
95 accumulation (Rodríguez-Vázquez et al., 2015). The metabolic signalling that allows the transfer of
96 storage lipids from adipocytes to ovaries is still incompletely understood. Here we identify CG3829
97 as one of the few of the 14 Drosophila SR-B that contain a conserved lipid binding residue
98 homologous to CD36. We show its role for the export of dietary lipids from the fat body to the
99 circulation. We named the protein Bez (**B**etween **E**mp and **Z**ip, pronounce "Beth") and found that in
100 Bez mutants, ovaries degenerate due to missing lipid transfer from the fat body. Bez mutant
101 adipocytes accumulate lipids and are unable to mobilize TG, and Bez-mediated lipid export from the
102 fat body is required to allow lipid accumulation during oocyte maturation. We demonstrate that Bez
103 transfers labeled lipids to the lipoprotein apoLpp, thereby distributing storage lipids to ovaries. We
104 thus establish a role for this SR-B in the metabolic regulation of reproduction.

105

106 **Results**

107 <u>The class B scavenger receptor Bez is expressed at the plasma membrane of adipocytes</u>

108 The *Drosophila* class B scavenger receptor (SR-B) Bez (CG3829) is one of 14 CD36-like protein family
109 members. We performed an Alphafold analysis of its predicted protein structure (Figure 1A). Similar
110 to human CD36, CG3829 contains two transmembrane domains and a large, extracellular barrel-like
111 putative lipid binding domain with high sequence similarity to CD36 (Supplemental Figure S1). Of
112 note, Bez is the only fly SR-B that contains two conserved lysine residues of the hydrophobic pocket
113 that in mammalian CD36 has been linked to lipid uptake (Kuda et al., 2013). The SR-B Peste (CG7228)
114 and Santa-maria (CG12789) contain one of these lysine residues, which are absent in the other
115 *Drosophila* SR-B. In addition, Bez contains two disorganized amino acid stretches at both termini. We
116 analyzed the expression pattern of the Bez protein in embryos and detected expression at the apical
117 membrane of the embryonic gut (Supplemental Figure S2A) and at the yolk sac (Supplemental Figure
118 S2B). Strong expression was also seen in the fat body (Figure 1B-D). In the embryonic fat body
119 (Figure 1B) marked by the lipid droplet surface protein Perilipin-1 (Plin1, Beller et al., 2010) Bez was
120 found primarily at the plasma membrane of the adipocytes (Figure 1C). To confirm this localization
121 we generated bez-RNAi clones in the fat body. Wildtype cells (GFP-negative) show high Bez
122 expression at the plasma membrane (illustrated by colocalization with the plasma membrane
123 protein alpha-Spectrin), while bez-RNAi clones (marked by the GFP signal) lacked Bez staining (Figure
124 1C, asterisks). Bez also localizes to the plasma membrane of the adult fat body adipocytes, marked
125 by Plin1 (Figure 1D). Taken together, the Bez expression pattern suggests a conserved function in
126 lipid uptake similar to that of CD36.

127 <u>Bez in the fat body is required for developmental timing</u>

128 To investigate the molecular function of Bez, we used a mutant where the P-element
129 P(EP)CG3829^{G8378} was inserted into the open reading frame (mutant allele *bez*^{EP}). By mobilizing this
130 EP element we generated a second allele (*bez*^{jo2}) featuring a stop codon in the sequence encoding
131 for the first transmembrane domain at the position of amino acid 89 (Figure 2A). The resulting Bez

132 mutants (*bez*$^{EP/jo2}$, bez-/-) do not express the Bez protein in embryos (Supplemental Figure S3). Bez
133 homozygous mutants are semi-viable, but females are sterile, and larvae show a strong
134 developmental delay. 50% of heterozygous controls pupariate after ~4,5 days at 25°C, while 50% of
135 homozygous Bez mutants pupariate at almost 6 days after egg laying (AEL). Similarly, adult flies
136 hatch ~1,5 days later than the heterozygous controls (Figure 2B). Expression of the UAS-Bez
137 construct in the fat body (*cg*-Gal4) reversed the developmental delay of Bez mutants (Figure 2B,
138 "rescue"). Next, we expressed RNAi against Bez in different tissues. Expression of Bez RNAi in the
139 midgut (*mex*-Gal4) or in hemocytes (*hml*-Gal4) did not phenocopy the developmental delay of Bez
140 homozygous mutants. By contrast, expression in the fat body (*cg*-Gal4) fully phenocopied the
141 developmental delay (Figure 2C). This shows that Bez function in the fat body is essential for normal
142 development.

143 Bez function in adipocytes is essential for female fertility

144 To analyze the cause for female sterility of Bez mutants, we investigated Bez mutant fecundity, egg
145 morphology, and ovary morphology. We found that Bez mutants lay fewer and smaller eggs and that
146 these eggs collapse, with no larvae hatching from them (Figure 3A). We dissected ovaries of control
147 females and Bez mutant females and found that also ovaries are small and degenerated (Figure 3B).
148 We then asked whether Bez was expressed in ovaries and performed quantitative real-time PCR of
149 RNA isolated from whole flies and from isolated ovaries (Figure 3C). We found that Bez is not
150 expressed in ovaries, suggesting that Bez functions remotely from the fat body to sustain ovary
151 maturation. We analyzed oogenesis by immunofluorescent staining of dissected ovaries and found
152 that oocyte maturation during oogenesis is blocked in Bez mutants: while control ovarioles contain
153 oocytes of all stages including mature eggs, Bez mutant ovarioles contain no mature eggs and no
154 oocytes older than stage 10. Localization of Orb, an RNA-binding protein that establishes polarity
155 during oogenesis (Lantz et al., 1994), was broader and less defined in the degenerated egg chambers
156 of Bez mutants (Figure 3D). Degenerated oocytes were apoptotic and showed fragmented DNA, as
157 shown by the fragmented DAPI staining. Next, we probed for the tissue-specific phenocopy of Bez
158 mutant fecundity. We found that expression of Bez RNAi in the fat body (*FB*-Gal4 or *cg*-Gal4) as well
159 as ubiquitous expression (*c355*-Gal4) is sufficient to block fecundity (Figure 3E). Expression of Bez
160 RNAi in the fat body (*FB*-Gal4 or *cg*-Gal4) was also sufficient to block oocyte maturation and to
161 induce oocyte apoptosis similar to Bez mutants (Figure 3F, Supplemental Figure S4A,B). Our results
162 show that Bez function in adipocytes is essential for oocyte maturation and thereby for female
163 fecundity.

164 Bez mutants are starvation-sensitive and do not mobilize triglyceride upon starvation

165 Oocytes display a shift in their lipid content between stage 8 and 10. Stage 10 oocytes store high
166 amounts of neutral lipids (Sieber & Spradling, 2015). To investigate if defects in lipid storage cause
167 ovary degeneration in Bez mutants, we stained neutral lipids with BODIPY. We confirmed that stage
168 10 oocytes massively take up storage lipids in heterozygous controls (Figure 3F, bez+/-).
169 Degenerated oocytes of homozygous Bez mutants did not contain increased amounts of neutral
170 lipids (Figure 3F, bez-/-). We quantified the fluorescence intensity of BODIPY in egg chambers
171 between stage 8 and 10, which showed that Bez homozygous mutant egg chambers do not increase
172 their lipid content (Figure 3H). This missing lipid uptake was phenocopied by expression of Bez RNAi
173 in the fat body (*cg*-Gal4, Figure 3G, H). By contrast, the stage 8 – stage 10 lipid transition was
174 independent from midgut expression of Bez: midgut depletion of Bez allowed for lipid accumulation,
175 and did not trigger egg chamber degeneration (*mex*-Gal4, Figure 3G, H). Next, we used a colorimetric
176 assay to measure triglycerides (TG) of whole female flies. Fat body-specific depletion of Bez by RNAi
177 led to significantly reduced total TG content compared to controls (Figure 4A).

178 We hypothesized that Bez is required for lipid mobilization from adipocytes, and that under Bez loss-
179 of-function, impaired lipid mobilization leads to insufficient lipid supply of oocytes. Lipid mobilization
180 as well as oocyte supply with lipids is strongly dependent on nutrient availability.

181 We thus asked if Bez mutants are unable to mobilize lipids upon starvation. Control female flies can
182 survive up to four days without food, with 50 % of flies surviving after 76 hours of starvation. Male
183 flies are less starvation-resistant with 50 % of flies surviving after 40 hours of starvation (Figure 4B).
184 Both female and male Bez mutants are significantly less starvation-resistant than controls. To
185 investigate if acute depletion of Bez from the fat body is sufficient to trigger starvation sensitivity,
186 we expressed Bez RNAi under the control of the temperature-sensitive Gal80 system in females. At
187 18°C, Gal80 expression suppresses Gal4 and thus the expression of bez-RNAi. At 29°C, Gal80 no
188 longer represses Gal4, allowing for the expression of bez-RNAi in the fat body. The resulting acute
189 depletion of Bez in adipocytes induced starvation sensitivity compared to controls (Figure 4C). Next,
190 we repeated the experiment and measured TG levels in whole male and female flies. At 18°C, the TG
191 content is reduced in response to nutrient restriction in both male and female flies (Figure 4D'). At
192 29°C, Bez depletion in adipocytes reduced the organismal TG content in both male and female flies
193 (Figure 4D'') and control flies reduced their TG content in response to nutrient restriction. TG levels
194 in male (Supplemental Figure S5A) and female (Figure 4D'') flies with Bez depletion in adipocytes
195 remained at similar levels under starvation. This shows that acute and adipocyte-restricted depletion
196 of Bez impairs lipid mobilization upon starvation.

197 <u>Bez loss-of-function alters lipid droplet size and lipid uptake into adipocytes</u>

198 We hypothesized that impaired lipid mobilization in Bez mutants would affect lipid droplet
199 morphology. We used larval fat body tissue of control animals and Bez mutants and stained lipid
200 droplets with BODIPY. The lipid droplet size was semi-quantified as the BODIPY-stained area (Figure
201 5A, B). Bez mutant fat body tissue contained significantly enlarged lipid droplets, while their number
202 per cell remained unchanged. Of note, this matched the lipid droplets phenotype in adipocytes of
203 loss-of-function mutants of Lipophorin (Lpp), a Drosophila lipoprotein homologous to ApoB (Palm et
204 al., 2012). We repeated the experiment in Bez mutant fat body tissue with Bez reconstituted in
205 distinct clones allowing for direct comparison of lipid droplet morphology within the same tissue
206 (Supplemental Figure 6A, B). Lipid droplet staining confirmed that these organelles are large in Bez
207 mutant adipocytes, while in adjacent rescue clones the droplets are small and more numerous.
208 Similarly, bez-RNAi leads to larger lipid droplets (Supplemental Figure S6C). Importantly,
209 overexpression of Bez using the UAS-Bez rescue construct did not alter lipid droplet morphology in a
210 wildtype background (Supplemental Figure S6D).

211 Next, we asked if the difference in lipid droplet morphology in Bez mutant fat body tissue
212 corresponds to differences in lipid content. We determined the total lipid content of isolated fat
213 body tissue of control and Bez mutant larvae by mass spectrometry (Figure 5C). Bez mutants
214 accumulate lipids of both types, the neutral lipids (DG, TG) and phospholipids (PE, PC, Supplemental
215 Figure 6E). To investigate how Bez affects uptake and incorporation of fatty acids into the lipidome
216 of the fat body we incubated isolated tissue of control flies and Bez mutants with alkyne-labeled
217 oleic acid (alkyne oleate, FA 19:1;Y) a traceable analog of the abundant natural oleic acid
218 (Kuerschner & Thiele, 2022). Upon click-reaction a mass spectrometry lipidome analysis was
219 performed (Wunderling et al., 2021). Bez mutants showed significantly increased total uptake and
220 incorporation of alkyne oleate into the TG pool generating labeled TG;Y (Figure 5D). Levels of labeled
221 phospholipids (PE;Y and PC;Y) were also elevated in the mutant tissue, but our measurements did
222 not reach significance. Taken together, this data shows that Bez mutant adipocytes enhance lipid

223 uptake and storage, but are unable to mobilize these lipids. This suggests that lipid export from
224 adipocytes to target tissues (such as oocytes) is impaired in Bez mutants.

225 Bez interacts with the apolipoprotein Lipophorin to distribute storage lipids

226 How does Bez affect the lipid content of oocytes without being present in ovaries? Lipids are
227 transported between organs by lipoproteins in both *Drosophila* and humans. A homolog of ApoB is
228 Rfabg/apoLpp (Lipophorin). We used a fly line that expresses Lpp fused to GFP under the control of
229 its endogenous promoter. We first analyzed if Bez colocalized with Lpp at the adipocyte plasma
230 membrane. Using airyscan super-resolution microscopy we found that both Bez and Lpp are
231 organized in distinct punctate domains at the adipocyte plasma membrane, several of which
232 colocalize (Figure 6A, Supplemental Figure 7A). Next, we asked if Bez has an impact on the lipid
233 composition of the lipoprotein particles. We isolated particles from Rfabg reporter animals of
234 wildtype or Bez mutant background and analyzed their lipid content by mass spectrometry. Although
235 similar in protein content (Figure 6B), particles from Bez mutants show a strongly reduced lipid
236 content, just missing statistical significance (Figure 6C). We then assessed the distribution of Lpp in
237 the gut and fat body. The apical membrane of the gastric caeca was marked by Lpp-GFP in control
238 animals, while in *Bez* mutants this membrane showed an even more intense signal (Figure 6D). In the
239 fat body, Lpp-GFP is found in a regular pattern at the plasma membrane of adipocytes, similar to the
240 Bez protein (Figure 6E). In the absence of Bez, this regular pattern is lost and Lpp-GFP presents in
241 aggregates at the plasma membrane.

242 Lipophorins were found to have a distinct fatty acid profile: in DG, medium-chain fatty acids (MCFA)
243 with an average chain length of 12-14 carbons are abundant, while in phospholipids, fatty acids with
244 an average chain length of 16-18 carbons are prevalent (Palm et al., 2012). Loading of MCFA-DG to
245 Lpp depends on transfer by lipid transfer particle (LTP) in the gut (Palm et al., 2012). We deepened
246 our mass spectrometry analysis of the Lpp lipid content by evaluating the fatty acid distribution
247 within the pools of DG and phospholipids (Supplemental Figure S7B). We confirmed the presence of
248 MCFA-DG and phospholipids with an average chain length of 16-18 carbons in isolated Lpp by mass
249 spectrometry. Strikingly, in Bez mutants a subpopulation of DG species containing medium-chain
250 fatty acids with chains of 12-14 carbons was found reduced and the total DG pool shifted towards
251 longer fatty acid chains (Supplemental Figure S7B). The fatty acid profile of phospholipids was also
252 slightly shifted, but fatty acids with an average chain length of 16-18 carbons remain the most
253 abundant species in phospholipids of Bez mutant Lpp. Together, this suggests that Bez might be
254 required for LTP/Lpp-mediated lipid export from the gut and for correct interaction of Lpp with the
255 adipocyte plasma membrane. However, knock-down of Bez in the gut did not trigger a
256 developmental delay or block oocyte maturation (Figure 2C, Figure 3G, H). We thus hypothesize that
257 interaction of Bez and Lpp in the fat body determines lipid delivery to oocytes and is limiting for
258 oocyte maturation.

259 Bez mediates lipid transfer from adipocytes to Lipophorin

260 As Bez localizes to the plasma membrane of adipocytes it becomes exposed to hemolymph and
261 lipoprotein particles. To corroborate the interaction of Lpp from the hemolymph with the membrane
262 receptor Bez, we isolated hemolymph from Lpp-GFP-expressing flies for incubation with Bez mutant
263 fat body tissue that contains Bez rescue clones (Figure 7A). In fat bodies incubated with hemolymph
264 from wildtype control flies, only background staining was visible in the GFP channel (Figure 7A,
265 upper panels). Alike, Bez mutant cells incubated with hemolymph from Lpp-GFP flies show only
266 minor signal for GFP (Figure 7A, lower panels). By contrast, the rescue clones show a strong staining

267 for apoLpp-GFP demonstrating a Bez-dependent recruitment of Lpp to the plasma membrane of
268 adipocytes.

269 We asked if the lipid transfer to Lpp by adipocytes depends on Bez. To address this question, we
270 used BODIPY to stain neutral lipids in control and Bez mutant fat bodies. Isolated Lpp-GFP particles
271 not containing any lipid dye were incubated for 60 min with the stained fat bodies. Upon removal of
272 the tissue the Lpp-GFP particles were analyzed by microscopy (Figure 7B). Lpp-GFP is visible as small,
273 GFP-positive aggregates. Lpp that were incubated with control fat body readily incorporated the
274 BODIPY dye. By contrast, Lpp exposed to fat body of Bez mutants showed a significantly reduced
275 BODIPY signal (Figure 7B, C). In a parallel set of experiments omitting the BODIPY stain we used the
276 alkyne oleic acid instead (Figure 7D). Here the different fat bodies were pre-incubated with tracer
277 yielding labeled lipid metabolites. After washing, the tissue was incubated for 60 min with naïve Lpp
278 before separation of tissue and Lpp. The particles were washed and analyzed by mass spectrometry
279 for their content of labeled lipids. As shown before (Figure 5D), Bez mutant adipocytes readily
280 incorporate alkyne oleate into their lipidome (Figure 7D, left). However, despite their elevated
281 content of labeled lipids, Bez mutant adipocytes struggle to transfer labeled lipids to Lpp (Figure 7D,
282 right). Accordingly, naïve Lpp incubated with Bez mutant tissue acquire relatively lower amounts of
283 labeled lipids: only ~6% were transferred, compared to ~20% for controls. Taken together, these
284 experiments show that Bez is required for productive lipid transfer from fat body to Lpp.

285 In sum, we suggest that Bez is required for lipid export from adipocytes, and that by interaction with
286 lipoproteins it regulates the distribution of lipids to ovaries, where these lipids are required for
287 oocyte maturation (Figure 7E). We thus demonstrate a role for a previously uncharacterized
288 scavenger receptor in the remote metabolic regulation of ovary development.

289

290 **Discussion**

291 The CD36 scavenger receptor plays a crucial role in fatty acid transport. CD36 is required to
292 incorporate dietary lipids into chylomicrons, which allows the transfer of fatty acids from the gut
293 into the circulation. Fatty acids transported by LDL are taken up into adipose tissue by LDL receptors,
294 and mobilization of lipids from adipocytes again requires CD36 (Daquinag et al., 2021). However,
295 whether CD36 interacts with lipoproteins in this process is unresolved yet. CD36 is also required for
296 adipogenesis, and patients with a CD36 deficiency show impaired chylomicron formation, reduced
297 lipid utilization and storage, and increased lipolysis (Zhao et al., 2018). Here we describe a novel role
298 for Bez, a largely uncharacterized CD36-like lipid scavenger receptor in lipid export from adipocytes
299 of *Drosophila melanogaster*. We show that in the absence of Bez, lipids accumulate in the fat body,
300 the major lipid-storing organ of *Drosophila* with functional homology to liver and adipose tissue.
301 Lipids are trapped in Bez mutant adipocytes, as becomes apparent by enlarged lipid droplets and by
302 an inability to mobilize lipids in response to starvation. Lipid export from storing tissue is not only
303 important to catabolize lipids for energy gain in times of nutrient scarcity, but also serves to nurse
304 target tissues such as imaginal discs, ovaries and the brain. The requirement of lipids for oocyte
305 development becomes apparent during maturation from stage 8 to stage 10 when oocytes
306 accumulate neutral lipids (Sieber & Spradling, 2015). Bez mutants are viable, but females are sterile
307 and lay very few, collapsed eggs. Bez mutant ovaries degenerate as apparent by the absence of
308 mature eggs and the presence of fragmented DNA in follicles from approximately stage 10 on as well
309 as the missing neutral lipid accumulation. Of note, it is sufficient to deplete Bez from the fat body to
310 reduce fecundity and induce starvation sensitivity. This highlights the importance of lipids stored in
311 adipocytes as dietary lipids directly from the gut cannot substitute. Bez is not expressed in ovaries,

312 which precludes a direct role for Bez in ovary lipidation, but further underlines its role in remote lipid
313 dispatch from the fat body.

314 Lipid transport through hemolymph is mainly mediated by Lipophorin (Lpp), a lipoprotein with ApoB
315 homology. ApoB is the characteristic apolipoprotein in human chylomicrons and low density
316 lipoprotein (LDL, Olofsson & Borèn, 2005). CD36 can interact with lipoproteins: an important
317 example is the role of CD36 as a receptor for oxidized LDL on macrophages. Upon binding of oxLDL
318 to macrophage CD36 in a blood vessel, the macrophages convert to foam cells and migrate into the
319 intima of the blood vessel, which marks the first step of a cascade leading to the formation of
320 atherosclerotic plaques (Libby, 2021). It is unclear to date if CD36 – lipoprotein interaction also
321 serves nutrient allocation in healthy individuals. We characterize one of the 14 Drosophila SR-Bs as a
322 mediator of storage lipid distribution. To this end, Bez interacts with Lpp. We show that Lpp
323 colocalizes with Bez at the adipocyte plasma membrane. Bez mutant adipocytes can no longer trap
324 Lpp at the plasma membrane. We show in two sets of experiments that lipid transfer from fat body
325 tissue to isolated Lpp is impaired in Bez mutants. BODIPY-stained lipids from wildtype fat body are
326 readily transferred onto exogenous, isolated Lpp; likewise, a traceable oleic acid analog (clickable
327 alkyne oleate) loaded on wildtypic fat body can be detected in Lpp upon incubation with the tissue.
328 We found considerably less BODIPY-stained lipids in Lpp that were incubated with Bez mutant fat
329 body tissue; moreover, while Bez mutant fat body accumulates lipids that incorporated alkyne
330 oleate, they transfer them at a lower rate to Lpp. Of note, we measured this in a time frame of 60
331 min, which leaves the possibility that lipid transfer is slower, but not completely abolished in Bez
332 mutants.

333 We propose the following model for the function of Bez: located to the plasma membrane of
334 adipocytes, but also gut cells, Bez mediates the export of lipids. The lipids are transferred to other
335 organs as energy source during nutrient scarcity or energy-demanding developmental processes. For
336 lipid mobilization, Bez interacts with Lpp the major lipid carrier in hemolymph that can also bind to
337 specific receptors in target organs such as oocytes. Lacking Bez, adipocytes fail to suffiently supply
338 lipids. Surprisingly, none of the other 8 SR-B (out of 14 family members) expressed in the fat body
339 (Herboso et al., 2011) can substitute; neither can intestinal Bez. To our knowledge, this study
340 describes a role in lipid export for one of these SR-B for the first time. Other SR-Bs are involved in the
341 uptake of their substrates, e.g. NinaD and Santa-maria in carotenoid uptake or Emp in endocytosis-
342 dependent protein uptake (Pinheiro et al., 2023). Our study suggests that Bez is also required for Lpp
343 interaction and lipid transfer from the gut, since Lpp accumulate in gastric caeca of Bez mutants.
344 While lipid export from gut cells might also be mediated by Bez, it does not affect oocyte
345 maturation. Midgut-specific depletion of Bez neither induces a developmental delay nor ovary
346 degeneration. This puzzling finding may relate to specific characteristics of the mobilized lipids.
347 Moreover, we show a reduced content of medium-chain DG in Lpp, which have been reported to
348 derive from the gut (Palm et al., 2012). The lipid export from gut cells might also be mediated by
349 Bez, but does not affect oocyte maturation. This is demonstrated by midgut-specific depletion of
350 Bez, which neither induces a developmental delay nor ovary degeneration. Dietary lipids are thus
351 insufficient to promote oocyte maturation. We speculate that lipids traffic sequentially and in a
352 coordinated way from the gut to the fat body, and upon remobilization further to different target
353 organs.

354 Our study opens the paths to several exciting research questions of inter-organ communication: how
355 are lipids sorted and allocated between gut, fat body and target tissues? Tissues like brain and
356 ovaries have completely different lipid compositions; how much does uptake of dietary lipids and
357 remodeling in the fat body contribute to their lipid signature? Is there a buffering system for the

358 incorporation of lipids of a specific chain lengths? For example, will dietary medium- or long chain
359 lipids affect the composition of ovary lipids, or be adjusted in the fat body? The combination of
360 *Drosophila* as a tractable genetic model that allows straightforward *in vivo* and *ex vivo* manipulation
361 of specific tissues with alkyne lipid tracing by high resolution and high content analysis is a promising
362 approach to answer these questions.

363

364 **Material and Methods**

365 Fly stocks, mutant generation and husbandry

366 The fly stocks used in this study were obtained from the Bloomington *Drosophila* Stock Center
367 (BDSC) at Indiana University: *bez*^{EP} (#28496), *w* (#6329), *c355-Gal4* (#3750), *cg-Gal4* (#7011), *lsp2-*
368 *Gal4* (#6357), *V32-Gal* (#4937), *prd-Gal4* (#1947), UAS-Dcr-2 (#24651), UAS-Flp (#4540), and
369 Ga4.Act5C (FRT.CD2) (#4780), and Gal4-Act5C (FRT.CD2), UAS-RFP (#30558); from the Vienna
370 Drosophila Resource Center (VDRC): the bez-RNAi lines *P(GD2224)v42872* (#42872) and
371 *P(KK111090)VIE-260B* (#103492) and the apoLpp-GFP line *PBac(fTRG00900.sfGFP-TVPTBF)VK00033*
372 (#318255) that expresses apoLpp tagged with sfGFP at the C-terminus; from the National Institute of
373 Genetics (NIG-FLY) at Japan the bez-RNAi line # 3829R-2. The group of Ronald Kühnlein (University of
374 Graz, Austria) kindly provided the stocks: *y*w*; P{w[+mW.hs]=GawB} FB P{w[+m*]UAS-*
375 *GFP1010T2}#2; P{w[+mC]=tubPGal80[ts]2* ; Sb1 e1 and *w*; P{w[*mW.hs]=GawB} FB; +*; and UAS-
376 Plin1-EGFP (w*;P{w+mC UAS-plin1::EGFP} / TM3).

377 The bez^{EP} allele has the EP-element P{w[+mC]=EP}CG3829[G8378] of 7.987 kb inserted in the third
378 exon of *bez* gene locus, 317 bp downstream of the translation initiation site ATG (Figure 2A). We
379 generate the null bez^{jo2} allele by mobilization of the EP-element that carries a mini-white gene [w^{+}].
380 Candidates were selected by loss of the mini-white transgene and by the sterility phenotype found in
381 homozygous bez^{EP} mutant females. PCR of genomic DNA of the bez^{jo2} allele showed that 35
382 nucleotides of the EP-element remained inserted in the Bez coding region and introduced a
383 premature termination code after amino acid 88. The apoLpp-GFP line was combined with the *bez*^{jo2}
384 allele to yield bez-/-; Lpp-GFP.

385 The genotype of the bez-RNAi stock used in this study is *w; UAS-bez*$^{3829R-2}$*; UAS-Dcr2, UAS-bez*^{GD2224}*.*
386 This line was generating by combination of the UAS-Dcr and two the bez RNAi lines: # 3829R-2 from
387 NIG and the bez RNAi line # 42872 from VDRC. Similar, but weaker phenotypes were obtained with
388 both independent RNAi lines, as well as with the VDRC line #103492.

389 The generation of the conditional bez-RNAi knockdown was done using the TARGET system
390 (McGuire, Mao, & Davis, 2004). The crosses between the Gal4 driver and the bez RNAi flies were
391 done at the restrictive temperature of 18°C, at which the Gal80 protein is active, represses Gal4 and
392 the UAS-bez-RNAi constructs are not expressed. Adult flies were collected in the first 24 hours after
393 eclosion, separated by sex and shifted to 29°C, temperature at which the Gal80 protein is inactive
394 and the UAS-bez-RNAi constructs start to be expressed. The flies were kept at 29°C for 4 days before
395 experiments were performed.

396 Clones in the fat body were generated by combining prd-Gal4 and UAS-Flp with an Actin-Gal4 STOP
397 cassette (Gal4-Act5C (FRT.CD2)) and UAS constructs. The prd enhancer is active during embryonic
398 development and drives the expression of the flipase that through the excision of a STOP cassette
399 allows the expression of the UAS constructs (the fluorescent reporters UAS-GFP or UAS-RFP and
400 UAS- bez-RNAi for knockdown or UAS-Bez for rescue experiments) independent from the original

401 prd enhancer. The prd-Gal4 has a transient, but very broad, expression pattern in cells that will
402 differentiate into fat body cells, which allow recovering many clones in adipocytes that have been
403 induced very early in development.

404 Generation of anti-Bez antibodies and Immunostainings

405 Anti-Bez antibody was generated after guinea pig immunization with the peptide
406 SHTKDAEMSMPARQESDR-Cys (amino acids: 2-19) at Pineda Antibody service (Berlin). The affinity
407 purified anti-Bez antibody was used at 1:100 dilution. The following additional primary antibodies
408 were used: rabbit anti-GFP (1:100; Santa Cruz), mouse anti-RFP (1:200; Santa Cruz), goat anti-E-
409 cadherin (1:100; Santa Cruz), rabbit anti-plin1 (1:100, gift from R. Kühnlein), mouse anti-α-spectrin
410 (1:10; 3A9, Developmental Studies Hybridoma Bank) and mouse anti-orb (1:100; 4H8 and 6H4 (1:1),
411 Developmental Studies Hybridoma Bank). Conjugated secondary antibodies Alexa488 (Molecular
412 Probes) and Cy3 (Jackson ImmunoResearch) were used at 1:200. Conjugated Alexa647 (Molecular
413 Probes) were used at 1:100. Stainings with DAPI, Nile Red, and BODIPY 558/588$_{C12}$ (Sigma Aldrich, D-
414 3835) were performed for 2 hours at room temperature during the incubation with the secondary
415 antibodies. Embryos were mounted in Fluoromount medium (Southern Biotech). Fluorescent images
416 were obtained on a Zeiss (LSM710) confocal microscope and Airyscan super-resolution were
417 obtained on a Zeiss LSM 880. Quantification of lipid droplet size and fluorescence intensities were
418 done with ImageJ. For colocalization analysis, we used the Plugin JACoP. For quantification of lipid
419 droplet size, we followed the protocol by (Ugrankar et al., 2019). Cells from 5 images from at least 3
420 different experiments were analyzed.

421 Molecular Biology and constructs

422 For pUAST-Bez generation, Bez coding sequence was amplified using the primers
423 CCGCGGCCGCTGATGTCACATACCAAAGATGCAGAG and GCTCTAGATTACGTTCCCTGATGGATGCCCCCA
424 from the GH19047 cDNA (Drosophila Genomics Resource Center (DGRC)) and inserted in pUAST by
425 using NotI and XbaI. Transgenic flies were generated using standard P-element transformation.

426 Quantitative real-time RT-PCR was performed with the iQ5 Real-Time PCR Detection System from
427 BIO-RAD, using the IQ SYBR Green Supermix (Biorad). The RNA was extracted using the NucleoSpin
428 RNA II kit (Machery & Nagel) and the cDNA were synthesized using the QuantiTect Reverse
429 Transcription Kit (Qiagen). cDNA samples were run in triplicates and experiments were repeated
430 with independently isolated RNA samples. The mRNA amounts were normalized to *rpL23 (rp49)*
431 mRNA values.

432 Quantification of egg deposition

433 For the quantification of egg depositions, crosses of a UAS-bez-RNAi line and different Gal4-driver
434 were performed with 10 females and transferred to 29 °C after 2 days. Eggs were collected in apple
435 juice agar plates coated with a thin layer of yeast in intervals of 24 hours. To determine production
436 rates the total number of eggs was counted over the following two days.

437 Starvation assay

438 For the starvation assay 20 four-day-old flies that were previously separated by sex were transferred
439 to starvation vials containing starvation medium (1 % agar in PBS) that only provide water supply.
440 Mortality rates were scored at 12-hour intervals by counting the number of dead flies as diagnosed
441 by the lack of sit-up response and finally determined as a percent of the total population. The

442 starvation assays with *bez*^{EP} mutants were performed at 25°C and for assays with conditional bez-
443 RNAi flies were maintained at 29°C.

444 Triglyceride measurements

445 Eight to ten adult flies were collected in 2 ml screw caps and frozen at -80°C. They were
446 homogenized in 600 µl PBT using the Precellys 24. After homogenization the tubes were centrifuged
447 at maximal speed at 4°C and the supernatant was transferred to a cold eppendorf tube (if necessary,
448 they were centrifuged a second time to remove debris). 10 µl were removed from the supernatant
449 and stored at -80°C in Eppendorf tubes for protein determination using the Pierce BCA Protein Assay
450 Kit. Protein content was calculated based on the albumin standard curve.

451 The remaining supernatant was heated for 10 min at 70°C and 20 µl of the heated supernatant, as
452 well as 20 µl glycerol standards (0.125, 0.25, 0.5 and 1 mg/ml) and a PBST blank, were transferred to
453 an eppendorf tubes in duplicates. To measure free glycerol, one of the samples was treated with 20
454 µl of PBT only and the other sample was treated with 20 µl of a triglyceride reagent (TGR). The TGR
455 contains a lipase, that digest the TAGs and relieves the glycerol backbone. In the next step, all the
456 probes were incubated for 45 min at 37°C. After incubation, the tubes were centrifuged for 3 min at
457 full speed (RT) and 30 µl of the probes and standards were transferred to a clear-bottom 96-well
458 plate and 100 µl of free glycerol reagent were added to each well using a multichannel pipette. The
459 plate was incubated at 37°C for 5 min sealed with parafilm. Air bubbles and condensate were
460 removed by centrifuging the plate. Absorbance at 540 nm was measured using a TECAN plate
461 reader.

462 To minimize errors, all the samples and standards were performed in triplicates. The average of the
463 triplicates was subtracted by the average of the blank. Triolein-equivalent standard curves were
464 constructed for the TGR-treated and untreated standards. Free glycerol content of the samples was
465 calculated based on these standard curves. Glycerol concentration of the TGR treated samples was
466 subtracted by the concentration of the untreated samples. The difference in glycerol concentration
467 hereby represents the amounts of TAGs that were digested by the enzymatic reaction. Finally, the
468 values were normalized to protein levels.

469 Hemolymph/Lipophorin purification and lipid extraction for lipidomics analysis

470 The hemolymph purification protocol was adapted from (Fernando-Warnakulasuriya & Wells, 1988).
471 40 third instar larvae were washed extensively in PBS to eliminate the food attached to the cuticle.
472 The larvae were homogenized in 250 µl of cold PBS containing protein inhibitors. The homogenate
473 was kept on ice for 5 min and then centrifuged at 3000 rpm at 4°C during 20 min. The supernatant
474 was transferred to a new tube avoiding taking the floating layer of fat and the cellular debris from
475 the pellet. The supernatant was centrifuged again at 1000 rpm for 20 min at 4°C. The supernatant
476 was transferred to a new tube and incubated immediately with dissected fat body. For lipidomics
477 analysis, lipids of 50 µl freshly isolated Lpp were extracted by addition of 100 µl LC-MS grade water.
478 500 µl extraction mix (5/1 MeOH/$CHCl_3$ (LC-MS grade) + 20 µL OMICS internal standard were added
479 as described (Thiele et al., 2019). Samples were sonicated for 30 min in a bath sonicator and
480 centrifuged for 2 min at 20000 g. The supernatant was decanted into a fresh tube. 300 µl $CHCl_3$ and
481 600 µl 1% acetic acid in LC-MS grade water were added. Samples were shaken manually for 10 s and
482 centrifuged at 20000 g for 5 min. The lower phase was transferred into a fresh tube and dried in a
483 speed-vac (Eppendorf concentrator plus) for 15 min at 45°C and redissolved in 500 µl spray buffer
484 (8/5/1 isopropanol/MeOH/H_2O (all LC-MS grade) + 10 mM ammonium acetate + 0.1% acetic acid
485 (LC-MS grade)) until mass spectrometry analysis.

486 BODIPY transfer to Lipophorin

487 Fat body tissue from control and Bez mutant larvae was dissected in triplicates in hemolymph-like
488 buffer (HL3A; 115 mM sucrose, 70 mM NaCl, 20 mM $MgCl_2$, 10 mM $NaHCO_3$, 5 mM KCl, 5 mM HEPES,
489 5 mM trehalose, pH 7.2 (Paradis et al., 2022)). Tissue was stained with BODIPY for 60 min. Fat body
490 tissue was washed extensively with HL3A to remove residual BODIPY. Lpp were isolated as described
491 in the preceeding paragraph and added 1/10 to the stained fat body. Lpp were incubated for 60 min
492 with the fat body on a nutator and fat body tissue was manually removed. Lpp were enriched by
493 centrifugation at 3000 g for 15 min, mounted in Fluoromount on a microscope slide and analyzed
494 immediately with a Zeiss LSM 710.

495 Alkyne lipid transfer analysis by mass spectrometry

496 A published protocol (Thiele et al., 2012) to preload Drosophila fat body tissue with alkyne oleate
497 was optimized. Click reaction and mass spectrometry analysis were as described (Thiele et al., 2019;
498 Wunderling et al., 2023). Briefly, fat body tissue from control and Bez mutant larvae was dissected in
499 triplicates in hemolymph-like buffer. Tissue was preloaded with 50 µM alkyne oleate (FA 19:1;Y) in
500 HL3A when incubated on a nutator for 60 min. An aliquot was taken to analyze the fat body lipidome
501 and quantify alkyne oleate uptake and metabolism. The remaining tissue was washed extensively
502 with HL3A to remove adherent alkyne lipid tracer. Isolated Lpp (see above) were added 1/10 to the
503 preloaded fat body tissue and incubated together on a nutator for 60 min. The fat body tissue was
504 carefully removed, first manually and then by passaging through a cell strainer. Flow-through was
505 centrifuged at 4°C and 3000 g for 15 min and the supernatant was removed. Lipids were extracted as
506 described above but additional internal standards for alkyne labelled metabolites were included
507 (Thiele et al., 2019). After drying of the sample, lipids were resolved in 10 µl $CHCl_3$ and sonicated for
508 5 min. 40 µl of C171 click mix (prepared by mixing 10 µl of 100 mM C171 in 50% MeOH (stored as
509 aliquots at −80°C) with 200 µl 5 mM Cu(I)$AcCN_4BF_4$ in AcCN and 800 µl ethanol) were added and the
510 samples were incubated at 40°C overnight (16 h). 200 µl $CHCl_3$and 200 µl water were added and the
511 samples were centrifuged at 20000 g for 5 min. The upper phase was discarded and samples were
512 dried in a speed-vac for 15 min at 45°C. Samples were resolved in 500 µl spray buffer and analyzed
513 by mass spectrometry.

514 Statistics

515 Bar charts represent mean and standard deviation. Error bars in curves represent standard error of
516 the mean (SEM). Boxes in box plots represent the interquartile range and median, whiskers
517 represent minimum and maximum. Green squares in box plots represent single data points. We
518 used Microsoft Excel and GraphPad Prism for bar charts and curves and Origin Pro 8G for box plots.
519 We used the software GraphPad Instat for our statistical analyses. Two-sided Student's t-test was
520 applied for normally distributed data in single comparisons, assuming heteroschedasticy. One-way
521 ANOVA with Tukey-Kramer post-test was used for multiple comparisons. The Kolmogorov-Smirnow
522 test was applied to test normality, and Bartlett's method was used to test for equal standard
523 deviations within groups. Asterisks represent * = $p < 0.05$, ** = $p < 0.01$, *** = $p < 0.001$. A minimum
524 of 3 biological replicates was used for each analysis.

525

526 **Author contribution**

527 Conceptualization: PC, LK, MHB; Methodology: PC, JO, LK, MHB; Investigation: PC, JO, YJ, KSR, LK,
528 MHB; Writing – Original Draft: PC, JO, MHB; Writing – Review & Editing: LK, PC, MHB; Visualization:
529 PC, MHB; Funding Acquisition: MHB; Supervision: PC, MHB.

530

531 **Acknowledgments**

532 We thank Darla Dancourt Ramos and Valeria Gulayeva for help with experiments and Almut Wingen
533 and Dominic Gosejacob for discussion. We thank Christoph Thiele for providing the alkyne oleate.
534 We thank Ronald Kühnlein for sharing the Plin1-GFP and Fat body-Gal4 fly line and Plin1 antibody.

535

536 **References**

537 Beller, M., Bulankina, A. V., Hsiao, H.-H., Urlaub, H., Jäckle, H., & Kühnlein, R. P. (2010). PERILIPIN-
538 Dependent Control of Lipid Droplet Structure and Fat Storage in Drosophila. *Cell Metabolism*,
539 *12*(5), 521–532. https://doi.org/10.1016/j.cmet.2010.10.001

540 Brown, M. S., Basu, S. K., Falck, J. R., Ho, Y. K., & Goldstein, J. L. (1980). The scavenger cell pathway
541 for lipoprotein degradation: Specificity of the binding site that mediates the uptake of
542 negatively-charged LDL by macrophages. *Journal of Supramolecular Structure*, *13*(1), 67–81.
543 https://doi.org/10.1002/jss.400130107

544 Canton, J., Neculai, D., & Grinstein, S. (2013). Scavenger receptors in homeostasis and immunity.
545 *Nature Reviews Immunology*, *13*(9), 621–634. https://doi.org/10.1038/nri3515

546 Daquinag, A. C., Gao, Z., Fussell, C., Immaraj, L., Pasqualini, R., Arap, W., … Kolonin, M. G. (2021).
547 Fatty acid mobilization from adipose tissue is mediated by CD36 posttranslational modifications
548 and intracellular trafficking. *JCI Insight*, *6*(17). https://doi.org/10.1172/jci.insight.147057

549 Dewett, D., Lam-Kamath, K., Poupault, C., Khurana, H., & Rister, J. (2021). Mechanisms of vitamin A
550 metabolism and deficiency in the mammalian and fly visual system. *Developmental Biology*,
551 *476*, 68–78. https://doi.org/10.1016/j.ydbio.2021.03.013

552 Fernando-Warnakulasuriya, G. J. P., & Wells, M. A. (1988). Isolation and characterization of
553 lipophorin fromDrosophila melanogaster larvae. *Archives of Insect Biochemistry and*
554 *Physiology*, *8*(4), 243–248. https://doi.org/10.1002/arch.940080405

555 Goldstein, J. L., Ho, Y. K., Basu, S. K., & Brown, M. S. (1979). Binding site on macrophages that
556 mediates uptake and degradation of acetylated low density lipoprotein, producing massive
557 cholesterol deposition. *Proceedings of the National Academy of Sciences*, *76*(1), 333–337.
558 https://doi.org/10.1073/pnas.76.1.333

559 GRUARIN, P., SITIA, R., & ALESSIO, M. (1997). Formation of one or more intrachain disulphide bonds
560 is required for the intracellular processing and transport of CD36. *Biochemical Journal*, *328*(2),
561 635–642. https://doi.org/10.1042/bj3280635

562 Guillou, A., Troha, K., Wang, H., Franc, N. C., & Buchon, N. (2016). The Drosophila CD36 Homologue
563 croquemort Is Required to Maintain Immune and Gut Homeostasis during Development and
564 Aging. *PLOS Pathogens*, *12*(10), e1005961. https://doi.org/10.1371/journal.ppat.1005961

565 Han, C., Song, Y., Xiao, H., Wang, D., Franc, N. C., Jan, L. Y., & Jan, Y.-N. (2014). Epidermal Cells Are
566 the Primary Phagocytes in the Fragmentation and Clearance of Degenerating Dendrites in
567 Drosophila. *Neuron*, *81*(3), 544–560. https://doi.org/10.1016/j.neuron.2013.11.021

568 Herboso, L., Talamillo, A., Perez, C., & Barrio, R. (2011). Expression of the Scavenger Receptor Class B
569 type I (SR-BI) family in Drosophila melanogaster. *The International Journal of Developmental*
570 *Biology*, *55*(6), 603–611. https://doi.org/10.1387/ijdb.103254lh

571 Heybrock, S., Kanerva, K., Meng, Y., Ing, C., Liang, A., Xiong, Z.-J., … Neculai, D. (2019). Lysosomal
572 integral membrane protein-2 (LIMP-2/SCARB2) is involved in lysosomal cholesterol export.
573 *Nature Communications*, *10*(1), 3521. https://doi.org/10.1038/s41467-019-11425-0

574 Krieger, M. (1997). The other side of scavenger receptors: pattern recognition for host defense.
575 *Current Opinion in Lipidology*, *8*(5), 275–280. https://doi.org/10.1097/00041433-199710000-
576 00006

577 Kuda, O., Pietka, T. A., Demianova, Z., Kudova, E., Cvacka, J., Kopecky, J., & Abumrad, N. A. (2013).
578 Sulfo-N-succinimidyl Oleate (SSO) Inhibits Fatty Acid Uptake and Signaling for Intracellular
579 Calcium via Binding CD36 Lysine 164. *Journal of Biological Chemistry*, *288*(22), 15547–15555.
580 https://doi.org/10.1074/jbc.M113.473298

581 Kuerschner, L., & Thiele, C. (2022). Tracing Lipid Metabolism by Alkyne Lipids and Mass
582 Spectrometry: The State of the Art. *Frontiers in Molecular Biosciences*, *9*.
583 https://doi.org/10.3389/fmolb.2022.880559

584 Ladanyi, A., Mukherjee, A., Kenny, H. A., Johnson, A., Mitra, A. K., Sundaresan, S., … Lengyel, E.
585 (2018). Adipocyte-induced CD36 expression drives ovarian cancer progression and metastasis.
586 *Oncogene*, *37*(17), 2285–2301. https://doi.org/10.1038/s41388-017-0093-z

587 Lantz, V., Chang, J. S., Horabin, J. I., Bopp, D., & Schedl, P. (1994). The Drosophila orb RNA-binding
588 protein is required for the formation of the egg chamber and establishment of polarity. *Genes*
589 *& Development*, *8*(5), 598–613. https://doi.org/10.1101/gad.8.5.598

590 Laugerette, F. (2005). CD36 involvement in orosensory detection of dietary lipids, spontaneous fat
591 preference, and digestive secretions. *Journal of Clinical Investigation*, *115*(11), 3177–3184.
592 https://doi.org/10.1172/JCI25299

593 Libby, P. (2021). The changing landscape of atherosclerosis. *Nature*, *592*(7855), 524–533.
594 https://doi.org/10.1038/s41586-021-03392-8

595 McGuire, S. E., Mao, Z., & Davis, R. L. (2004). Spatiotemporal Gene Expression Targeting with the
596 TARGET and Gene-Switch Systems in *Drosophila*. *Science's STKE*, *2004*(220).
597 https://doi.org/10.1126/stke.2202004pl6

598 Nichols, Z., & Vogt, R. G. (2008). The SNMP/CD36 gene family in Diptera, Hymenoptera and
599 Coleoptera: Drosophila melanogaster, D. pseudoobscura, Anopheles gambiae, Aedes aegypti,
600 Apis mellifera, and Tribolium castaneum. *Insect Biochemistry and Molecular Biology*, *38*(4),
601 398–415. https://doi.org/10.1016/j.ibmb.2007.11.003

602 Olofsson, S. -O., & Borèn, J. (2005). Apolipoprotein B: a clinically important apolipoprotein which
603 assembles atherogenic lipoproteins and promotes the development of atherosclerosis. *Journal*
604 *of Internal Medicine*, *258*(5), 395–410. https://doi.org/10.1111/j.1365-2796.2005.01556.x

605 Osz, K., Ross, M., & Petrik, J. (2014). The thrombospondin-1 receptor CD36 is an important mediator
606 of ovarian angiogenesis and folliculogenesis. *Reproductive Biology and Endocrinology*, *12*(1),
607 21. https://doi.org/10.1186/1477-7827-12-21

608 Palm, W., Sampaio, J. L., Brankatschk, M., Carvalho, M., Mahmoud, A., Shevchenko, A., & Eaton, S.
609 (2012). Lipoproteins in Drosophila melanogaster—Assembly, Function, and Influence on Tissue
610 Lipid Composition. *PLoS Genetics*, *8*(7). https://doi.org/10.1371/journal.pgen.1002828

611 Paradis, M., Kucharowski, N., Edwards Faret, G., Maya Palacios, S. J., Meyer, C., Stümpges, B., …
612 Bülow, M. H. (2022). The ER protein Creld regulates ER-mitochondria contact dynamics and
613 respiratory complex 1 activity. *Science Advances*, *8*(29).
614 https://doi.org/10.1126/sciadv.abo0155

615 Pinheiro, A. S., Tsarouhas, V., Senti, K. A., Arefin, B., & Samakovlis, C. (2023). Scavenger receptor
616 endocytosis controls apical membrane morphogenesis in the Drosophila airways. *ELife*, *12*.
617 https://doi.org/10.7554/eLife.84974

618 Plüddemann, A., Neyen, C., & Gordon, S. (2007). Macrophage scavenger receptors and host-derived
619 ligands. *Methods*, *43*(3), 207–217. https://doi.org/10.1016/j.ymeth.2007.06.004

620 Rigotti, A., Acton, S. L., & Krieger, M. (1995). The Class B Scavenger Receptors SR-BI and CD36 Are
621 Receptors for Anionic Phospholipids. *Journal of Biological Chemistry*, *270*(27), 16221–16224.
622 https://doi.org/10.1074/jbc.270.27.16221

623 Rodríguez-Vázquez, M., Vaquero, D., Parra-Peralbo, E., Mejía-Morales, J. E., & Culi, J. (2015).
624 Drosophila Lipophorin Receptors Recruit the Lipoprotein LTP to the Plasma Membrane to
625 Mediate Lipid Uptake. *PLOS Genetics*, *11*(6), e1005356.
626 https://doi.org/10.1371/journal.pgen.1005356

627 Sieber, M. H., & Spradling, A. C. (2015). Steroid Signaling Establishes a Female Metabolic State and
628 Regulates SREBP to Control Oocyte Lipid Accumulation. *Current Biology*, *25*(8), 993–1004.
629 https://doi.org/10.1016/j.cub.2015.02.019

630 Silverstein, R. L., & Febbraio, M. (2009). CD36, a Scavenger Receptor Involved in Immunity,
631 Metabolism, Angiogenesis, and Behavior. *Science Signaling*, *2*(72).
632 https://doi.org/10.1126/scisignal.272re3

633 Silvestris, E., Lovero, D., & Palmirotta, R. (2019). Nutrition and Female Fertility: An Interdependent
634 Correlation. *Frontiers in Endocrinology*, *10*. https://doi.org/10.3389/fendo.2019.00346

635 Talamillo, A., Herboso, L., Pirone, L., Pérez, C., González, M., Sánchez, J., … Barrio, R. (2013).
636 Scavenger Receptors Mediate the Role of SUMO and Ftz-f1 in Drosophila Steroidogenesis. *PLoS*
637 *Genetics*, *9*(4), e1003473. https://doi.org/10.1371/journal.pgen.1003473

638 Thiele, C., Papan, C., Hoelper, D., Kusserow, K., Gaebler, A., Schoene, M., … Kuerschner, L. (2012).
639 Tracing Fatty Acid Metabolism by Click Chemistry. *ACS Chemical Biology*, *7*(12), 2004–2011.
640 https://doi.org/10.1021/cb300414v

641 Thiele, C., Wunderling, K., & Leyendecker, P. (2019). Multiplexed and single cell tracing of lipid
642 metabolism. *Nature Methods*, *16*(11). https://doi.org/10.1038/s41592-019-0593-6

643 Ugrankar, R., Bowerman, J., Hariri, H., Chandra, M., Chen, K., Bossanyi, M.-F., … Henne, W. M.
644 (2019). Drosophila Snazarus Regulates a Lipid Droplet Population at Plasma Membrane-Droplet
645 Contacts in Adipocytes. *Developmental Cell*, *50*(5), 557-572.e5.
646 https://doi.org/10.1016/j.devcel.2019.07.021

647 Wingen, A., Carrera, P., Ekaterini Psathaki, O., Voelzmann, A., Paululat, A., & Hoch, M. (2017). Debris
648 buster is a Drosophila scavenger receptor essential for airway physiology. *Developmental*
649 *Biology*, *430*(1), 52–68. https://doi.org/10.1016/j.ydbio.2017.08.018

650 Wunderling, K., Leopold, C., Jamitzky, I., Yaghmour, M., Zink, F., Kratky, D., & Thiele, C. (2021).
651 Hepatic synthesis of triacylglycerols containing medium-chain fatty acids is dominated by
652 diacylglycerol acyltransferase 1 and efficiently inhibited by etomoxir. *Molecular Metabolism*,
653 *45*, 101150. https://doi.org/10.1016/j.molmet.2020.101150

654 Wunderling, K., Zurkovic, J., Zink, F., Kuerschner, L., & Thiele, C. (2023). Triglyceride cycling enables
655 modification of stored fatty acids. *Nature Metabolism*, *5*(4), 699–709.
656 https://doi.org/10.1038/s42255-023-00769-z

657 Zhao, L., Varghese, Z., Moorhead, J. F., Chen, Y., & Ruan, X. Z. (2018). CD36 and lipid metabolism in
658 the evolution of atherosclerosis. *British Medical Bulletin*, *126*(1), 101–112.
659 https://doi.org/10.1093/bmb/ldy006

660

661

662 **Figures and Figure legends**

Figure 1

A Alphafold protein structure prediction of CD36 and Bez

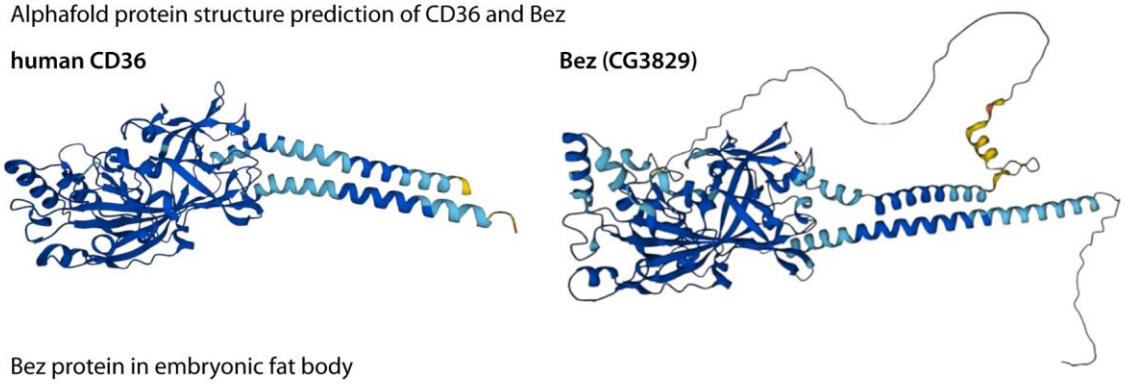

B Bez protein in embryonic fat body

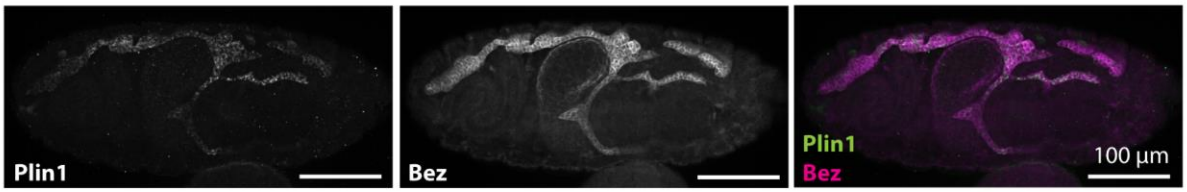

C Bez protein at the plasma membrane of larval adipocytes

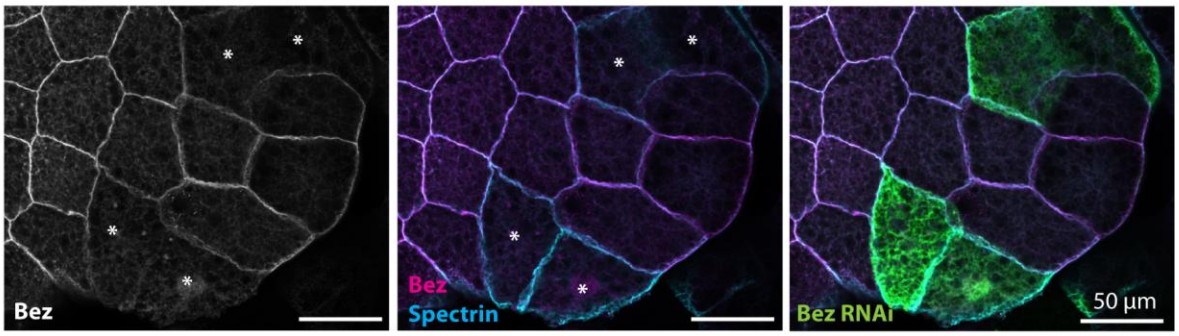

D Bez protein in adult fatbody

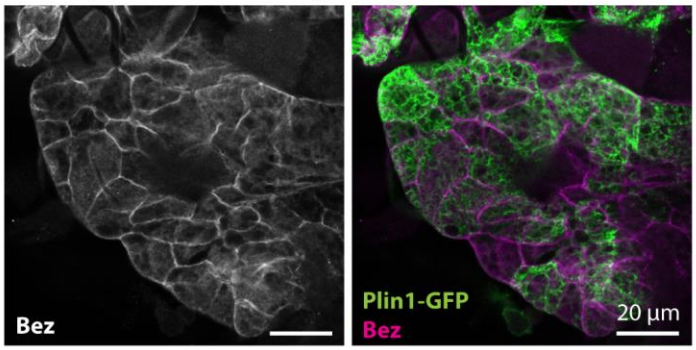

663

664 Figure 1: The class B scavenger receptor Bez is expressed at the plasma membrane of adipocytes

665 A) Protein structure prediction by Alphafold of human CD36 (Platelet glycoprotein 4) and *Drosophila*
666 *melanogaster* CG3829 (Bez) shows the N- and C-terminal transmembrane domains and the
667 extracellular, barrel-formed lipid transport domain of CD36. The two transmembrane domains and
668 the extracellular, putative lipid transport domain are conserved in *D. melanogaster*. In addition, Bez
669 has two disorganized amino acid stretches at the N- and C-terminus.

670 B) The Bez protein is expressed in the embryonic fat body: Confocal images of embryos show co-
671 expression of Bez and the lipid droplet protein Plin1. Representative images from 5 independent
672 replicates. Scale bars represent 100 µm.

673 C) The Bez protein is expressed at the plasma membrane of larval fat body cells. Confocal images of
674 3rd instar larval fat body shows colocalization of Bez with the membrane marker alpha-Spectrin.
675 Clones expressing bez-RNAi are marked with GFP and show no Bez staining in the plasma
676 membrane. Representative images from 5 independent replicates. Scale bars represent 50 µm.

677 D) Bez is expressed at the plasma membrane of adult fat body. Plin1-GFP was expressed in
678 adipocytes using cg-Gal4. Representative images from 5 independent replicates. Scale bars
679 represent 20 µm.

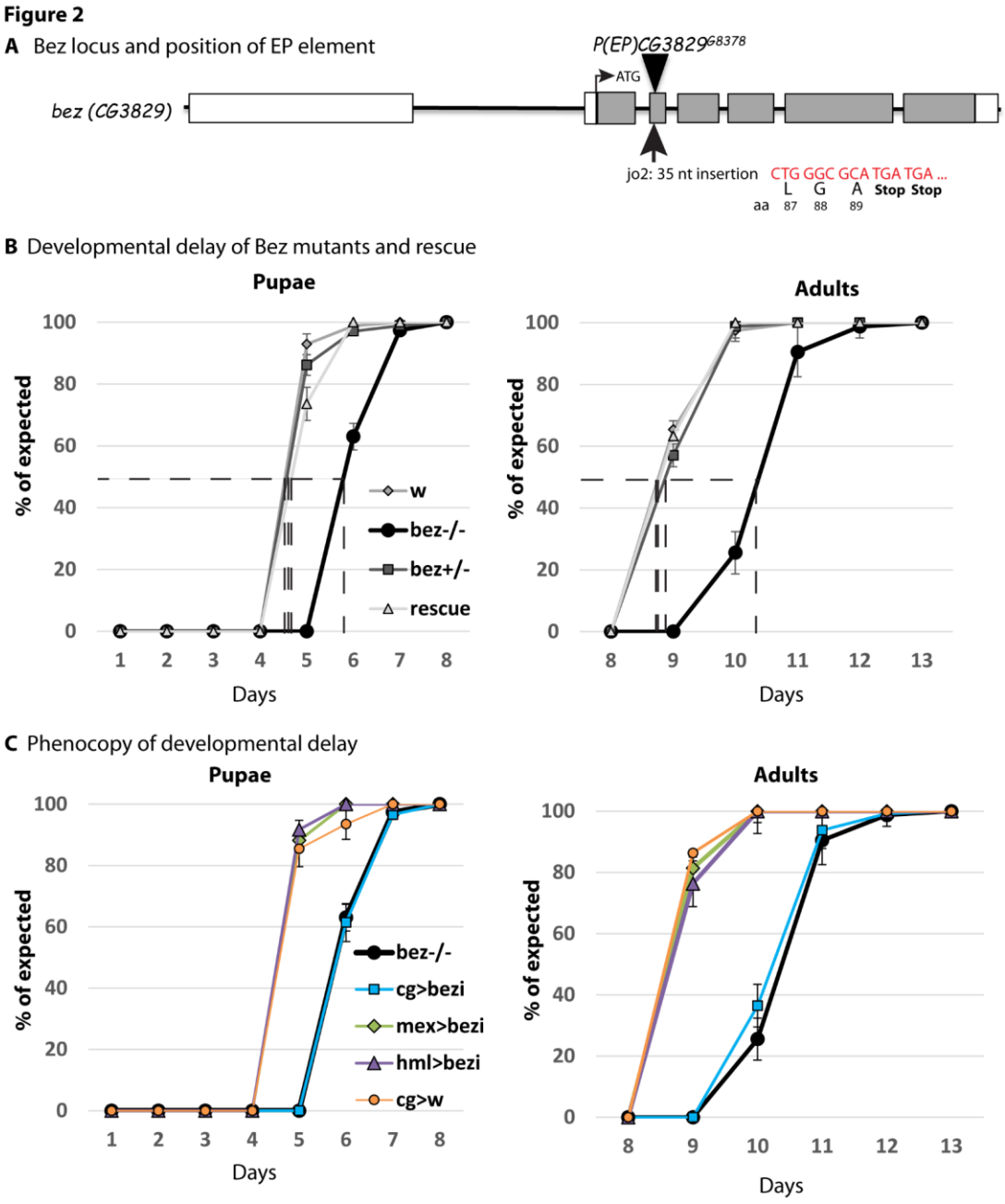

Figure 2: Bez is required in the fat body for developmental timing

A) Representation of the *bez* locus and the position of the EP element that mutate the *bez* locus and was used to create an additional jump-out (jo2) allele. Nucleotide insertion contained in the jo2 allele is shown in red. The 35 nt insertion yields two stop codons after amino acid 89.

B) Bez mutant development is delayed by >1 day. 50% of heterozygous controls pupariate after 4.5 days at 25°C while homozygous mutants pupariate after 5.75 days. Adult hatching is similarly delayed, with 50% of heterozygous controls hatching after 9 days and homozygous mutants after 10.3 days. Developmental delay is rescued by expression of UAS-Bez in the fat body (*cg*-Gal4). Error bars represent SEM. n=5 in groups of 20 individuals.

C) The delay in pupal and adult development is phenocopied by knocking down Bez in the fat body (cg-Gal4, blue line, control in orange) by RNAi, but not in the midgut (mex-Gal4, green line) or in hemocytes (hml-Gal4, purple line). Error bars represent SEM. n=5 in groups of 20 individuals.

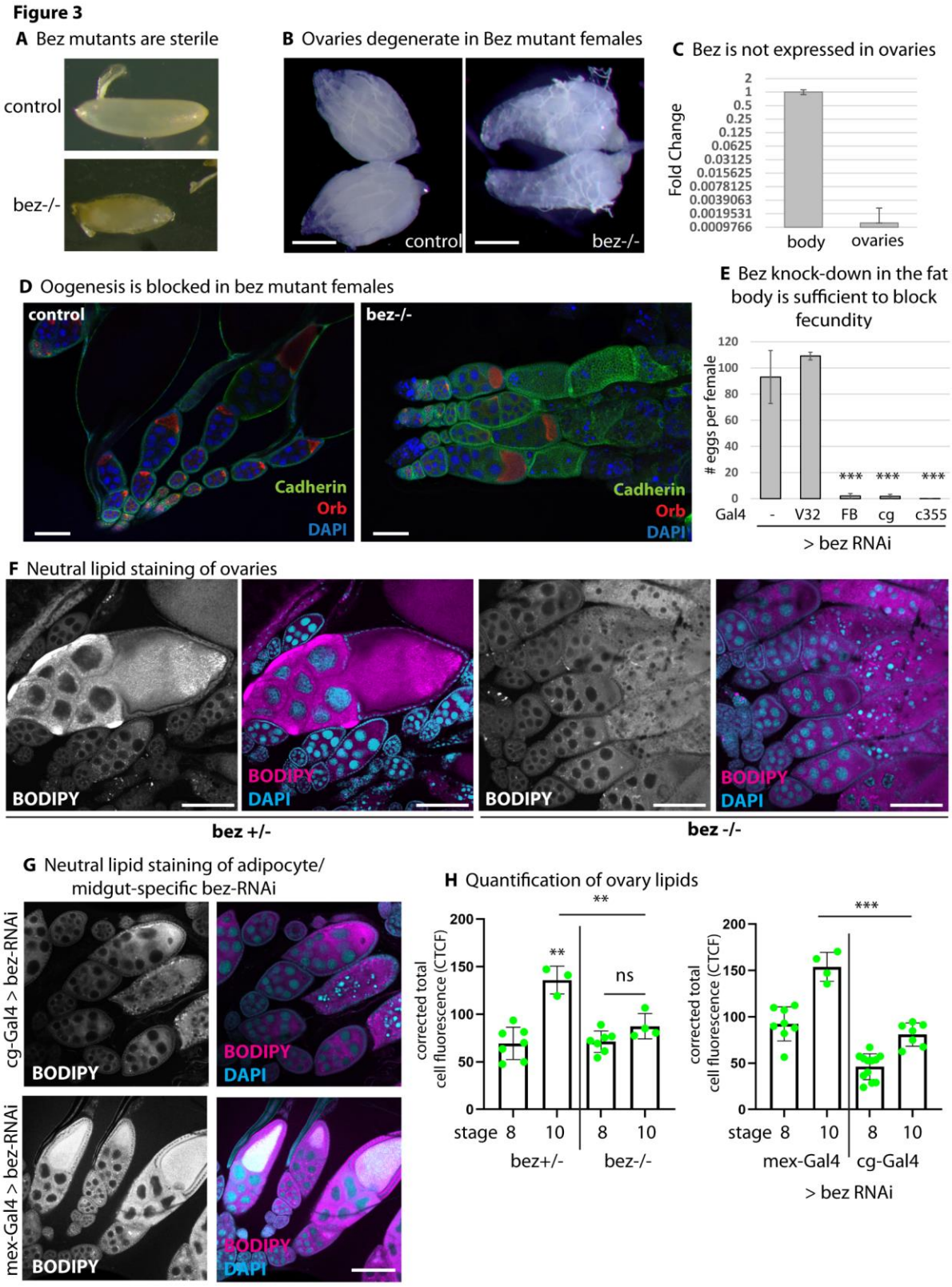

693

694 Figure 3: Bez function in adipocytes is essential for female fertility

695 A) Bez mutant females are sterile and lay unviable, collapsed eggs. Representative images from 10
696 independent replicates.

697 B) Bez mutant female ovaries degenerate. Representative images from 10 independent replicates.
698 Scale bars represent 250 µm.

699 C) The *bez* transcript is not expressed in ovaries. Quantitative real-time PCR from isolated ovaries
700 compared to whole females. Scale bars represent standard deviation. Mean of 8 experiments.

701 D) Oogenesis is blocked in Bez mutants. Confocal images show wildtype and Bez mutant ovaries
702 stained with anti-E-Cadherin, anti-Orb and DAPI. Bez mutant oocytes do not mature into eggs.
703 Representative images from 10 independent replicates. Scale bars represent 100 µm.

704 E) Knock-down of Bez by RNAi in the fat body (*FB*-Gal4, *cg*-Gal4 and *c355*-Gal4) is sufficient to block
705 fecundity, while knock-down of Bez in germ line (*V32*-Gal4) cells has no effect. n=5 in groups of 20
706 individuals. Asterisks represent *** $p > 0.001$.

707 F) Bez mutant ovaries do not store lipids. Neutral lipid staining (BODIPY) shows lipid accumulation in
708 stage $\geq$ 10 ovaries in heterozygous controls, but not in homozygous Bez mutants.

709 G) Bez RNAi knock-down in the fat body (*cg*-Gal4) is sufficient to reduce the lipid content of ovaries.
710 Bez RNAi knock-down in the midgut (*mex*-Gal4) does not block lipid accumulation on ovaries and
711 does not induce oocyte degeneration. Representative images from 5 independent replicates. Scale
712 bars represent 100 µm.

713 H) Quantification of fluorescence intensity of BODIPY from F and G. Asterisks represent *** $p >$
714 0.001, ** $p > 0.01$, ns: not significant.

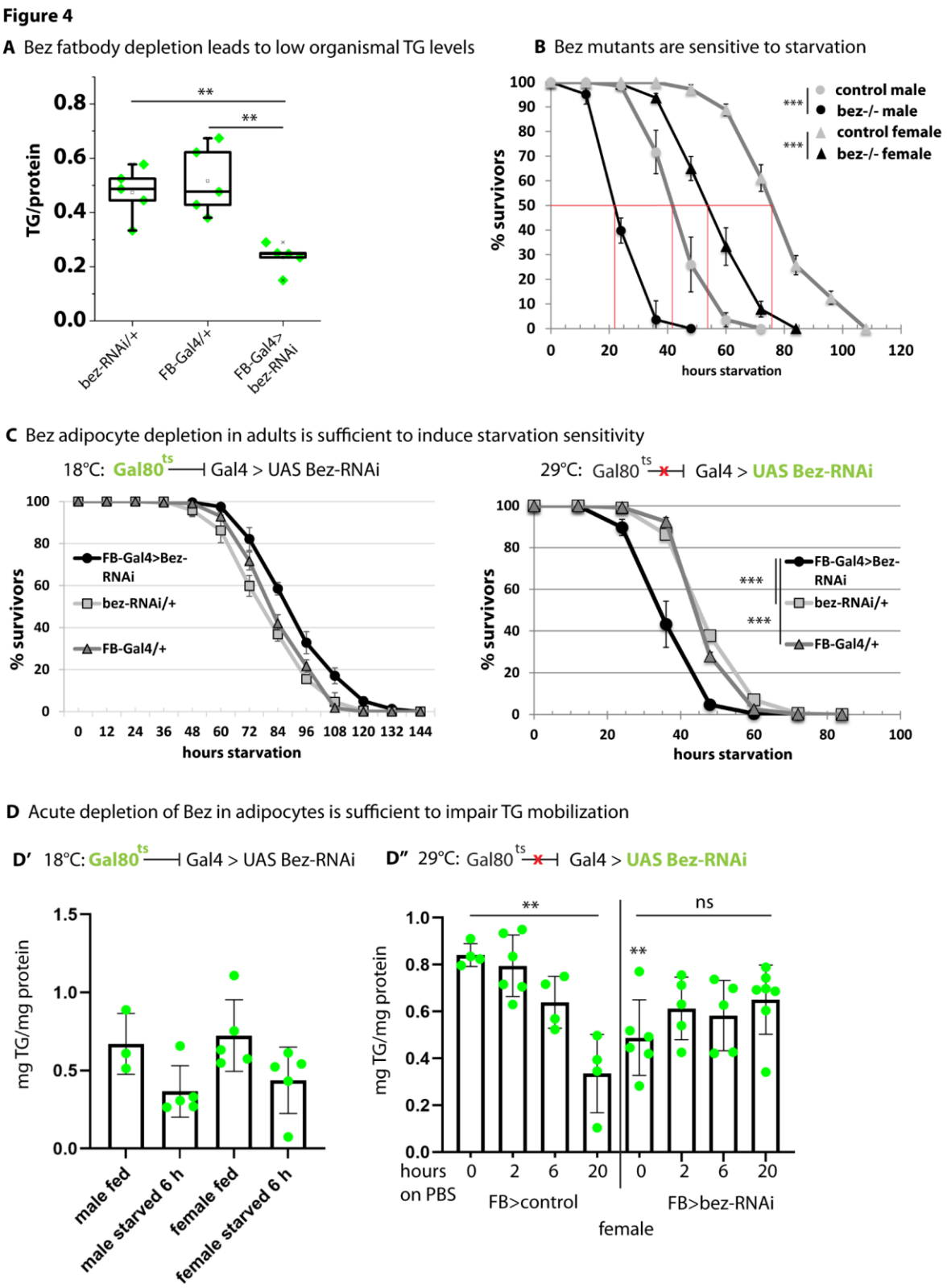

Figure 4: Bez mutants are starvation-sensitive and fail to mobilize lipids

A) RNAi knock-down of Bez in the fat body (*FB*-Gal4) reduces the levels of the storage lipid triacylglycerol as determined by a colorimetric assay. n=5 in groups of 8-10 individuals. Asterisks represent ** $p > 0.01$.

720 B) Bez mutants are sensitive to starvation. 50 % of wildtype female flies are dead after ~75 hours
721 under food deprivation while 50 % of Bez mutants are dead after ~50 h. Male flies have lower
722 starvation resistance: 50 % wildtypes are dead after ~40 h and ~20 h in Bez mutants. Flies were kept
723 at 25 °C. n=5 in groups of 20 individuals. Asterisks represent *** $p > 0.001$.

724 C) Adult onset of Bez fat body depletion is sufficient to induce starvation sensitivity in females,
725 suggesting that it is due to lipid mobilization defects rather than storage of lipids. bez-RNAi was
726 expressed in the fat body (*FB*-Gal4). The thermosensitive Gal80 inhibitor was blocked in adults at 29
727 °C, leading to Bez depletion and starvation sensitivity. n=5 in groups of 20 individuals. Asterisks
728 represent *** $p > 0.001$.

729 D) Triacylglycerol (TG) as determined by a colorimetric assay from whole flies expressing bez RNAi in
730 the fat body (*FB*-Gal4) under the control of the inducible Gal4/Gal80 system. At 18 °C, Gal4 is
731 inactive and both male and female flies can mobilize TG upon starvation (D'). At 29 °C, Gal4 is active
732 and drives the expression of bez-RNAi (D'', right side) in female flies. In controls, FB Gal4/Gal80^{ts} was
733 crossed to wildtype (D'', left side). Depletion of Bez from the fat body blocks TG reduction upon
734 starvation. n $\geq$ 3 in groups of 8 individuals. Asterisks represent ** $p > 0.01$, ns: not significant.

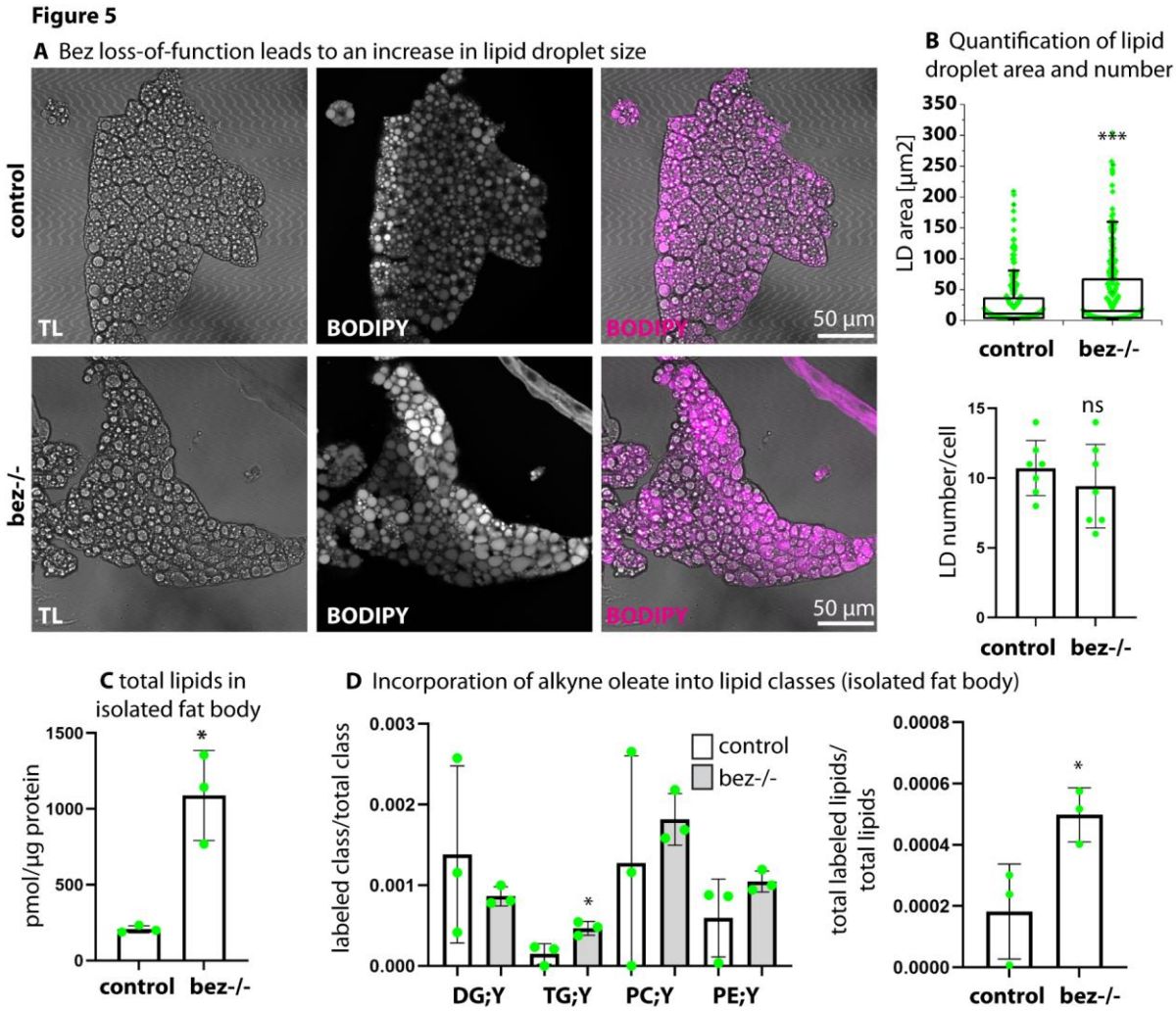

735

736 Figure 5: Bez loss-of-function affects lipid droplet size and lipid uptake

737 A) Confocal images show control (w-) and Bez mutant adipocytes in fat body tissue. TL: transmission
738 light. Lipid droplets are stained with BODIPY. Bez mutant cells show increased lipid droplet size.
739 Representative images from 10 independent replicates.

740 B) Quantification of lipid droplet size (area) and number per cell. Asterisks represent *** $p > 0.001$,
741 ns: not significant.

742 C) Lipid content of 5 isolated fat bodies determined by mass spectrometry and normalized to protein
743 content. n = 3. Asterisk represents * $p > 0.05$.

744 D) Incorporation of alkyne oleate (FA19:1;Y) into lipid classes as determined by click reaction
745 followed by mass spectrometry. Shown are incorporation into diacylglycerol (DG;Y), Triacylglycerol
746 (TG;Y), phosphatidylglycerol (PC;Y), phosphatidylethanolamine (PC;Y) and total lipids. n = 3. Asterisk
747 represents * $p > 0.05$.

748

749 Figure 6: Bez interacts with the apolipoprotein apoLpp

750 A) Larval fat body cells from Rfabg (apoLpp)-GFP expressing animals (under the control of an
751 endogenous promoter). Airyscan confocal images with the endogenous Bez scanned in the AiryScan
752 mode show Lpp-GFP and Bez colocalization at the plasma membrane of adipocytes. Images show
753 single confocal section. Representative images from 5 independent replicates. Scale bar as indicated.

754 B) Protein content of isolated Lpp fraction of control and Bez mutant larvae. n = 3.

755 C) Lipid content of isolated Lpp fraction as determined by mass spectrometry and normalized to
756 protein. n = 3.

757 D) Confocal images of larval anterior midgut showing gastric caeca and proventriculus (PV) of Lpp-
758 GFP and Lpp-GFP; Bez-/- larvae. Representative images from 5 independent replicates. Scale bar as
759 indicated.

760 E) Confocal images of larval fat body of Lpp-GFP and Lpp-GFP; Bez-/-. Lpp localizes in a regular
761 pattern at the plasma membrane and colocalizes with Bez in controls. In Bez mutants, Lpp forms
762 aggregates and no longer marks the plasma membrane. Representative images from 5 independent
763 replicates. Scale bars as indicated.

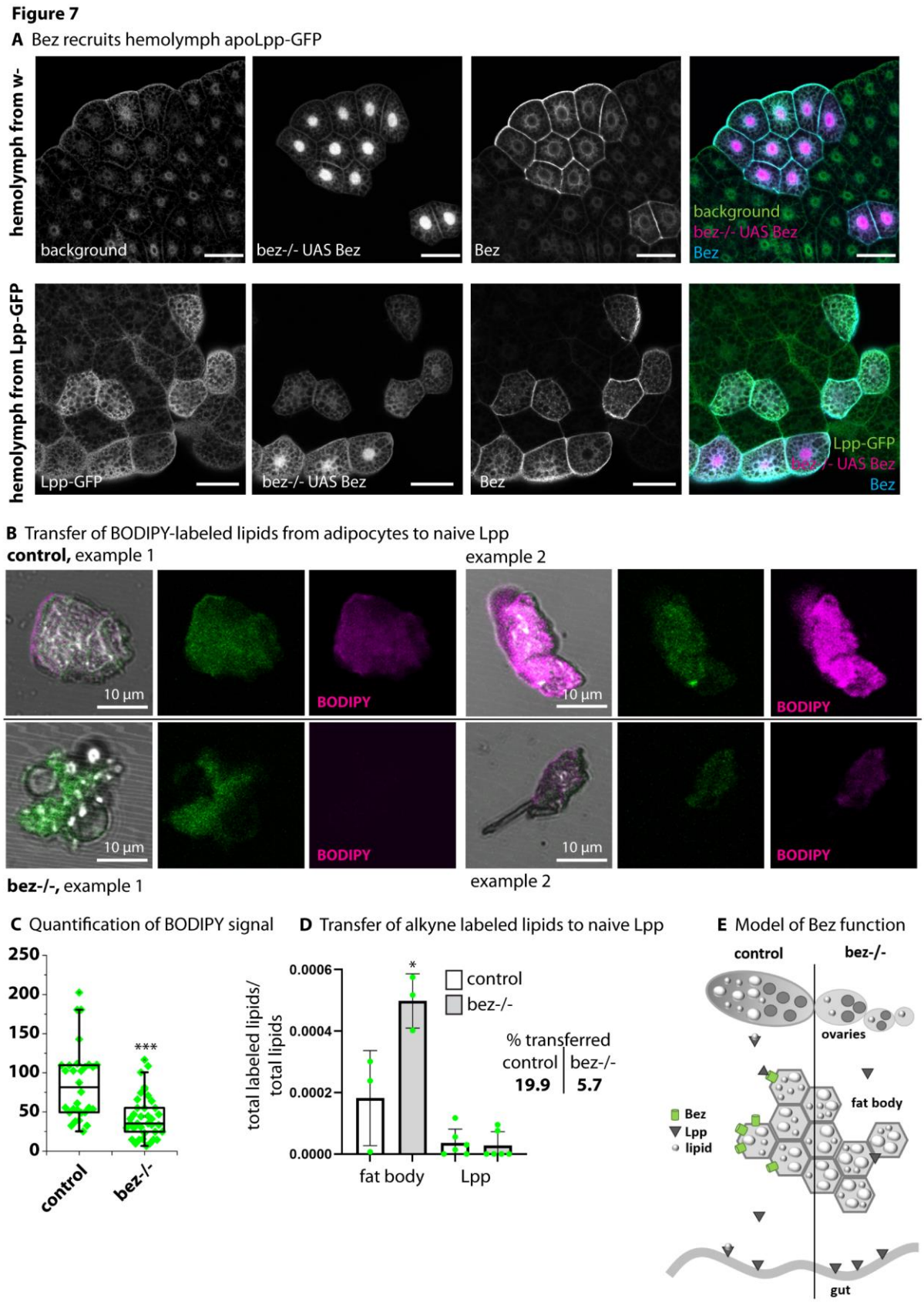

764

765 Figure 7: Bez is required for lipid transfer from adipocytes to Lpp

766 A) Bez can recruit the lipoprotein Rfabg (apoLpp, CG11064) to adipocytes. The upper panel shows
767 the control that was incubated with hemolymph from w- controls. Bez rescue clones are labeled

with RFP, RFP-negative cells are bez-/-. The lower panel shows bez-/- fat body tissue that was incubated with hemolymph from Lpp-GFP-expressing flies. Bez rescue clones are marked with RFP. Bez-/- show only background staining for Lpp-GFP, while rescue clones strongly bind Lpp. Representative images from 5 independent replicates. Scale bars represent 50 µm.

B) Confocal images of Lpp-GFP aggregates. Lpp from the Rfabg line that expresses Lpp-GFP under its endogenous promoter were incubated with BODIPY-stained fat body from controls and Bez mutants. BODIPY is readily transferred from control adipocytes to naïve Lpp (upper panel, two examples are shown). Transfer of BODIPY-labeled lipids is absent (example 1) or reduced (example 2) from Bez mutant adipocytes. Representative images from 5 independent replicates. Scale bars as indicated.

C) Quantification of the BODIPY fluorescence intensity in Lpp aggregates from B. Asterisks represent *** $p > 0.001$.

D) Transfer of clicked alkyne oleate as determined by mass spectrometry. Lpp from the Rfabg line that expresses Lpp-GFP under its endogenous promoter were incubated with alkyne oleate-loaded fat body from controls and Bez mutants. Bez mutant adipocytes incorporate more alkyne oleate than control adipocytes, but hardly transfer the traceable analog to Lpp.

E) Model of Bez function: in the presence of Bez, lipids can be transferred from adipocytes to Lpp and distributed to ovaries. Lipids accumulate in the fat body and ovaries cannot mature in Bez mutants.

Supplement

Protein sequence alignment of human CD36 and Bez (CG3829)

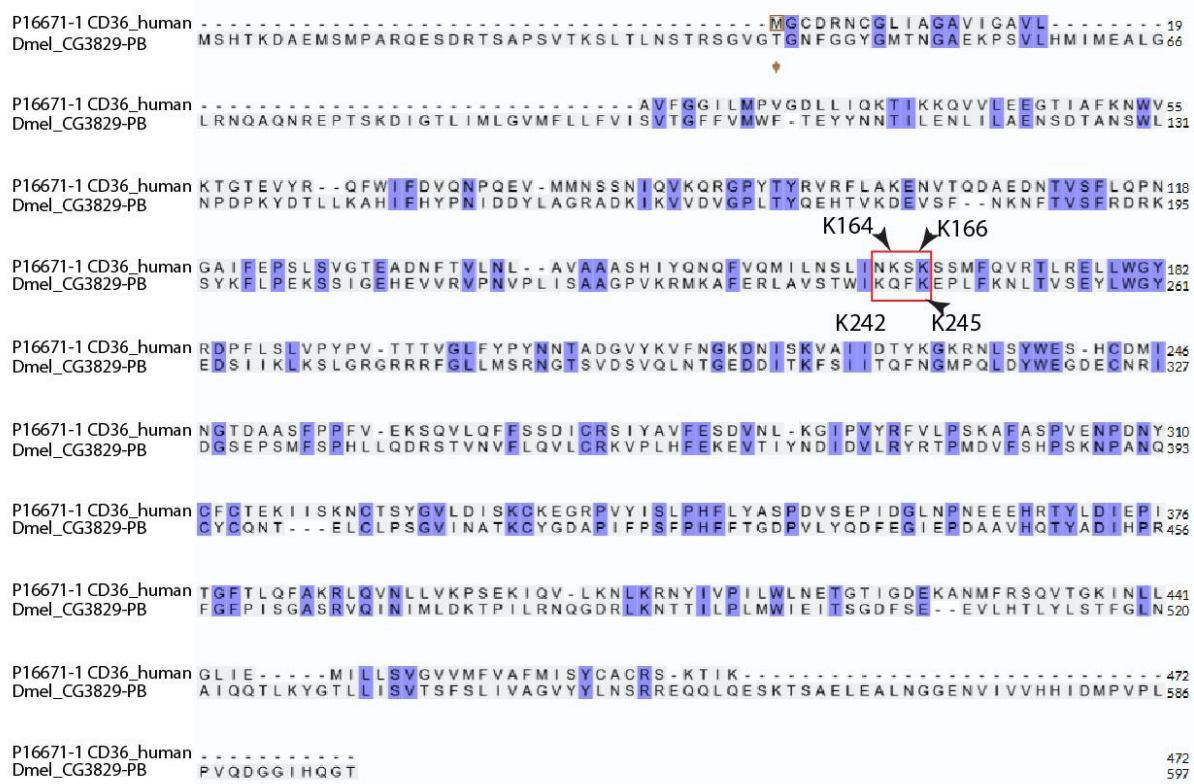

790 Supplemental Figure S1: Protein sequence alignment of human CD36 and *D. melanogaster* CG3829
791 shows several conserved regions and the additional N- and C-terminal amino acid stretches of Bez.
792 Lysine residues of the lipid binding pocket are marked in red.

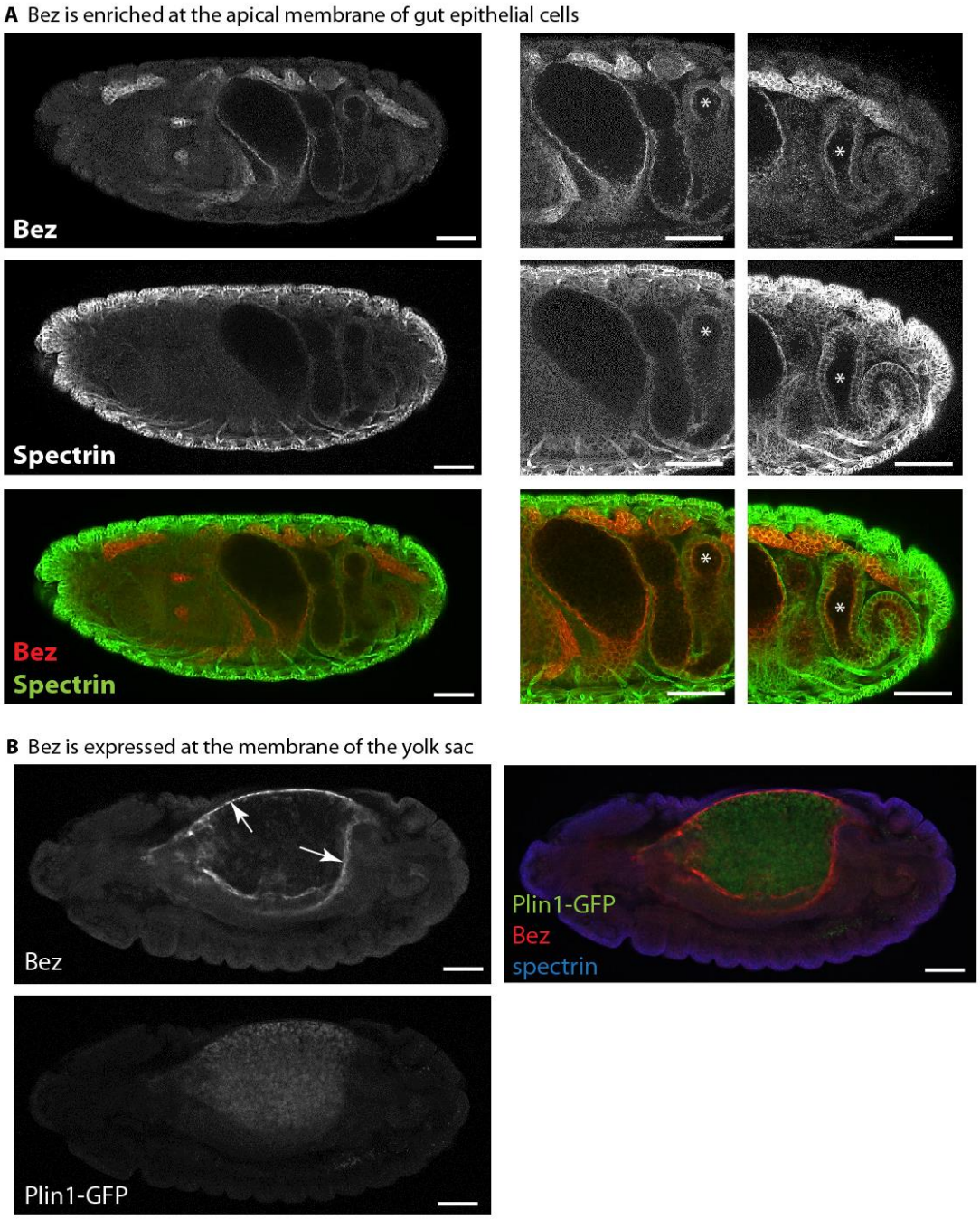

793

794 Supplemental Figure S2: A) In addition to embryonic fat body, Bez is expressed in the gut, where it is
795 enriched in the apical membrane. B) Bez is expressed at the yolk sac. Scale bars represent 50 µm.

796

797

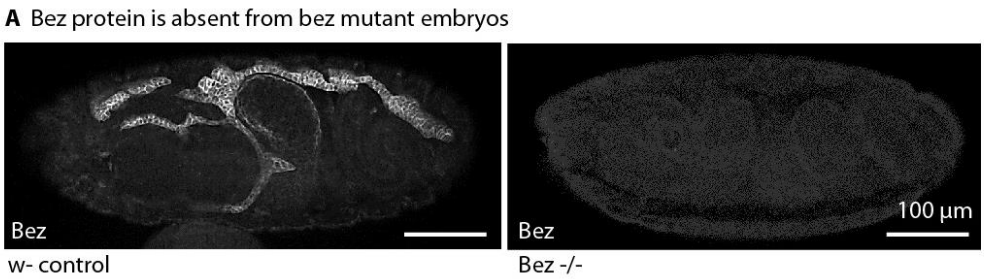

Supplemental Figure S3: Bez protein is absent from Bez mutant embryos. Confocal images show wildtype and Bez mutant embryos stained with anti-Bez. Scale bars represent 100 µm.

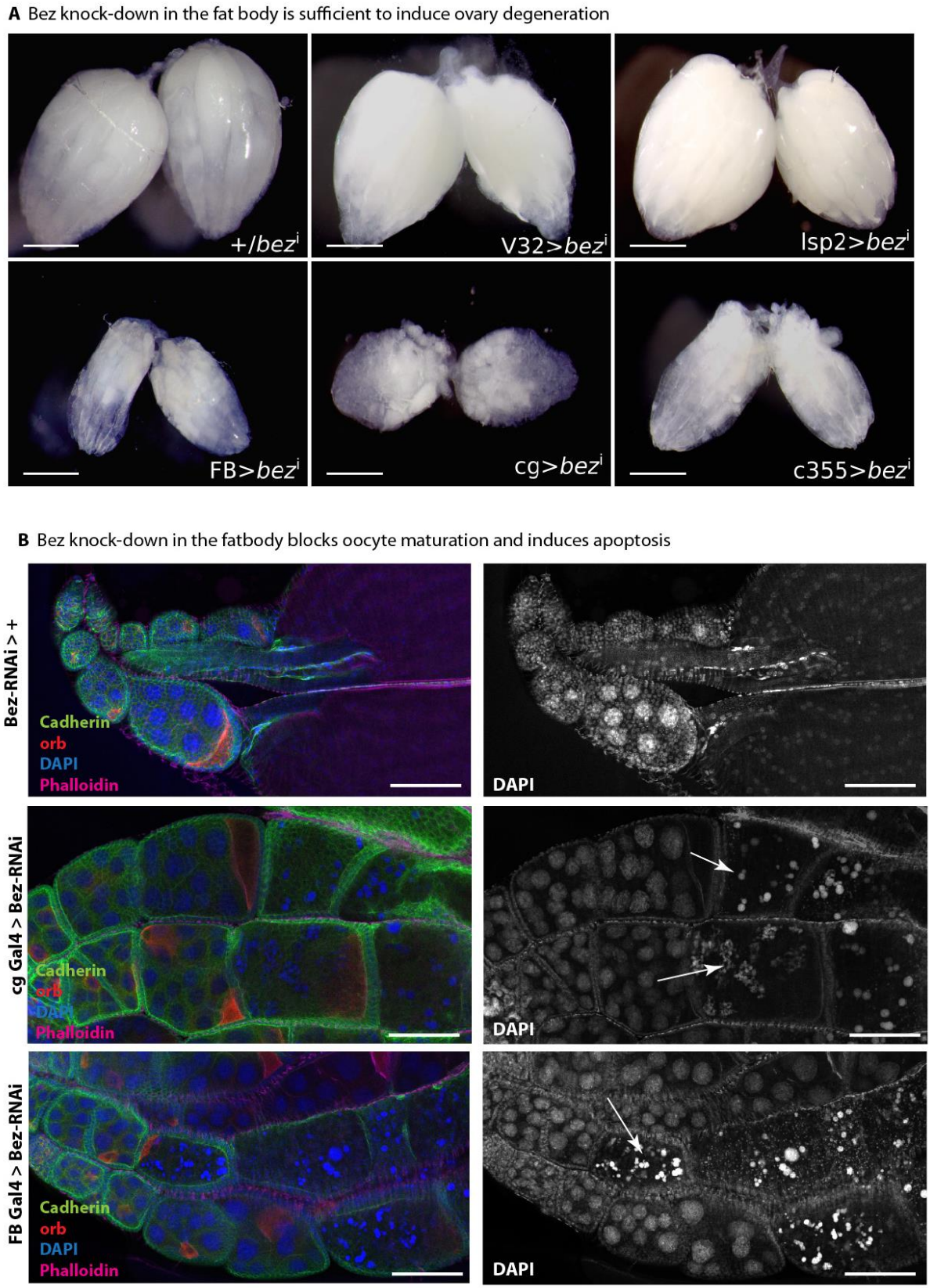

Supplemental Figure S4: A) bez-RNAi-mediated knock-down is sufficient to induce ovary degeneration. Upper panel from left to right: control without driver; Germline-specific driver (*V32*-Gal4) or hemolymph-specific driver (*lsp2*-Gal4) do not induce ovary degeneration. Lower panel: Fat body-specific knock-down of Bez (*FB*-Gal4, *cg*-Gal4, *c355*-Gal4) induces egg chamber degeneration.

806 B) Knock-down of Bez by RNAi in the fat body (*FB*-Gal4 and *cg*-Gal4) blocks oocyte maturation and
807 induces apoptosis. Mature eggs are absent in fat body-specific bez-RNAi (2nd and 3rd panel) and DNA
808 is fragmented (arrows). Representative images from 5 independent replicates. Scale bars represent
809 100 µm.

810

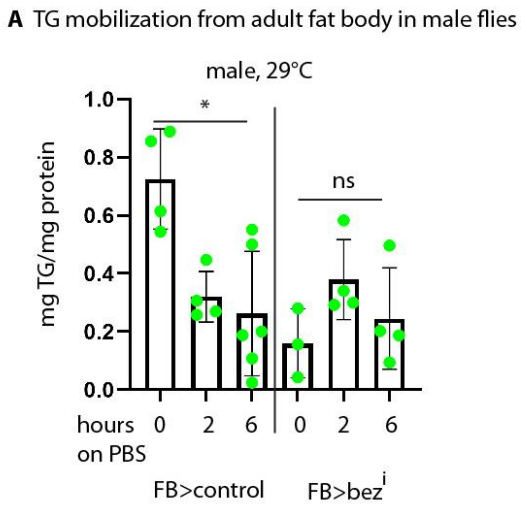

811

812 Supplemental Figure S5: A) Triacylglycerol (TG) as determined by a colorimetric assay from whole
813 male flies expressing bez- RNAi in the fat body (*FB*-Gal4) under the control of the inducible
814 Gal4/Gal80 system. At 29 °C, Gal4 is active and drives the expression of bez-RNAi (right side). In
815 controls, FB Gal4/Gal80^{ts} was crossed to wildtype (left side). Depletion of Bez from the fat body
816 blocks TG reduction upon starvation in male flies. n $\geq$ 3 in groups of 8 individuals. Asterisks represent
817 * $p > 0.05$, ns: not significant.

818

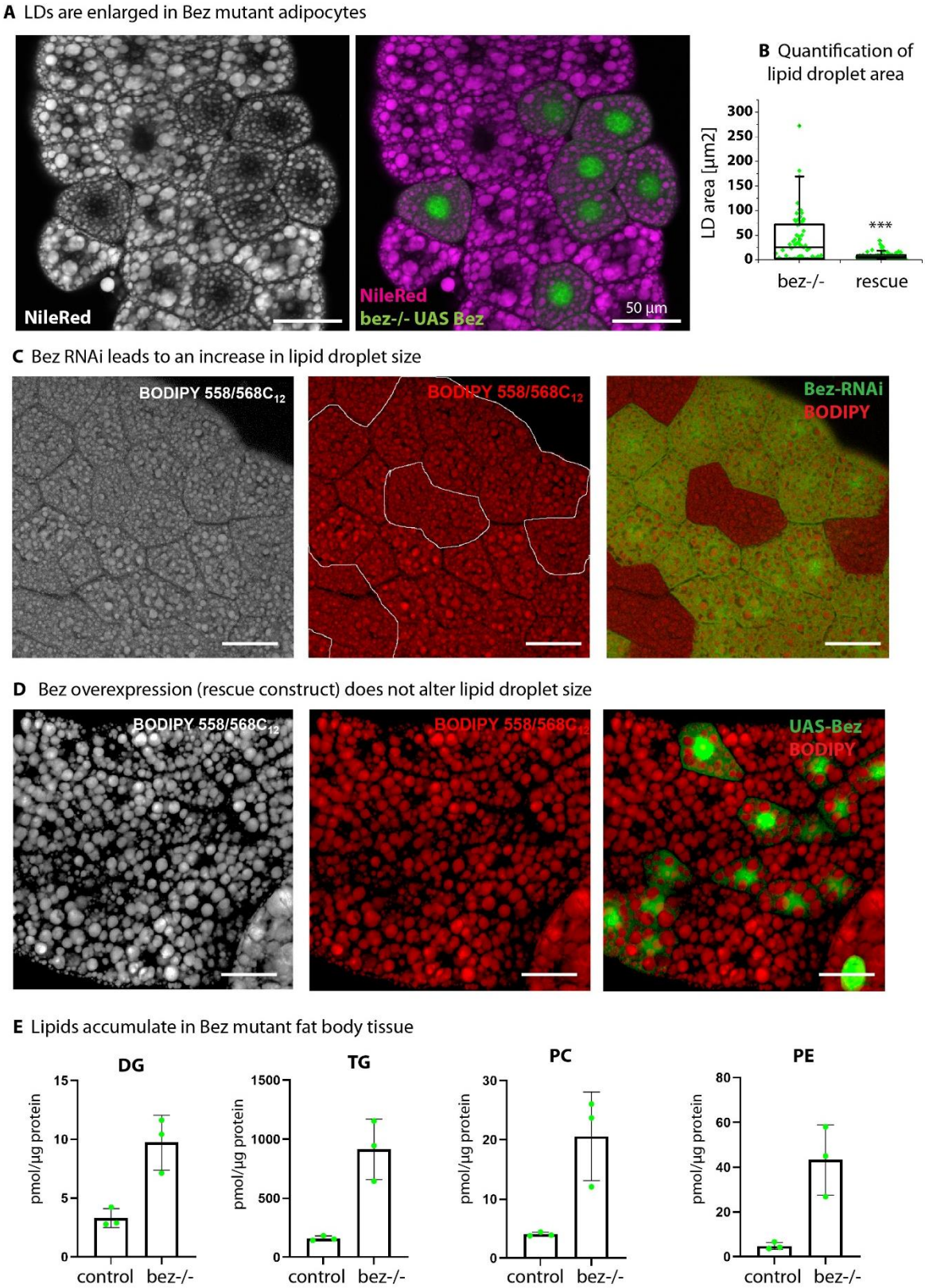

Supplemental Figure S6: A) Confocal images show Bez mutant adipocytes with rescue clones marked with GFP. Lipid droplets are stained with NileRed. Bez mutant cells show increased lipid droplet size. Representative images from 10 independent replicates. B) Quantification of lipid droplet size (area). Asterisks represent *** $p > 0.001$. C) Fat body clones expressing Bez RNAi show increased LD size similar to bez-/- adipocytes. Lipids stained with BODIPY. Scale bars represent 50 µm. D) Bez

825 overexpression in a wildtype background has no effect on LD size. Lipids stained with BODIPY. Scale
826 bars represent 50 µm. E) Selected lipid classes as determined by mass spectrometry. DG:
827 diacylglycerol, TG: triacylglycerol, PC: phosphatidylglycerol, PE: phosphatidylethanolamine.

828

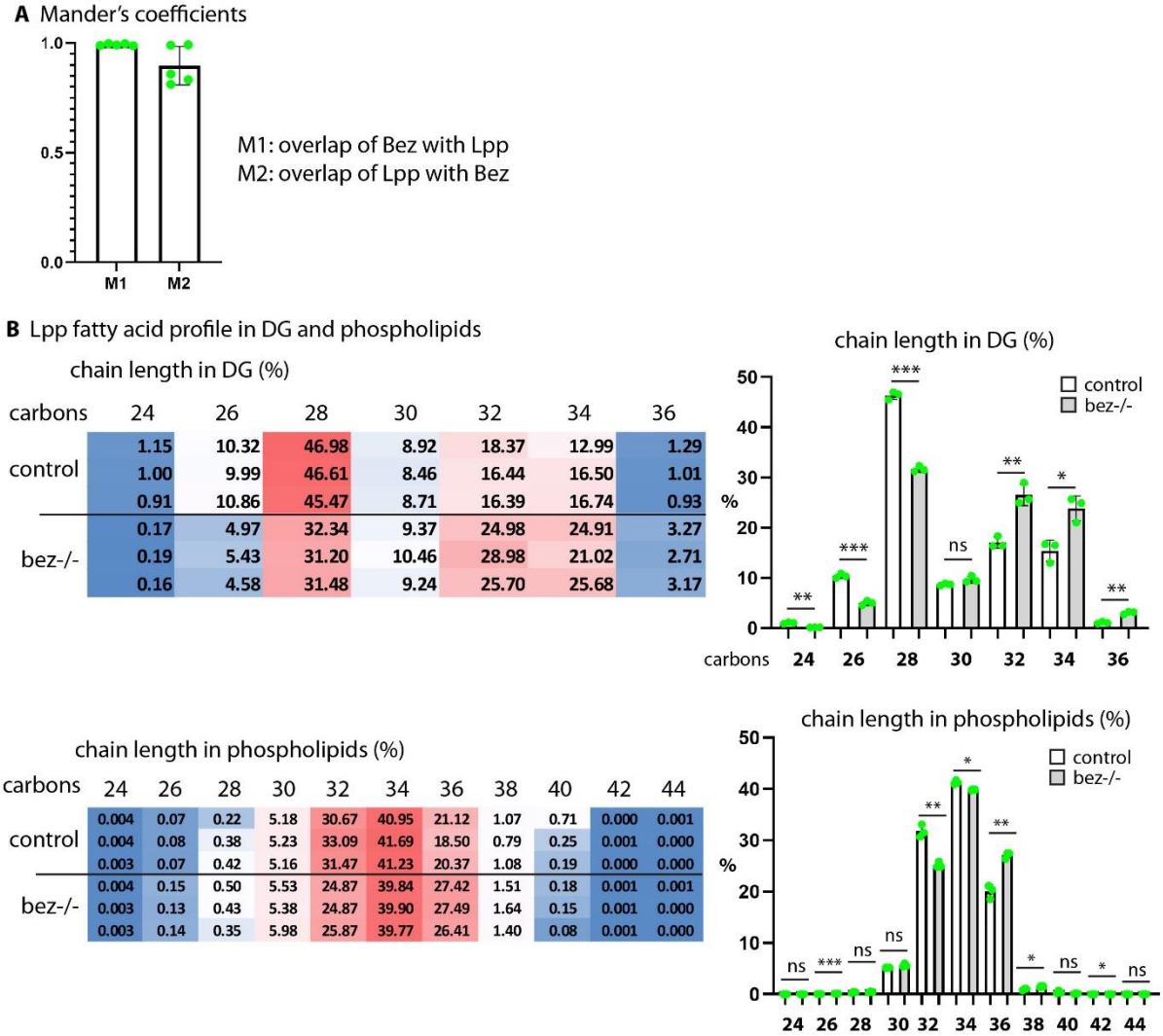

829

830 Supplemental Figure S7: A) Mander's coefficient for colocalization analysis of Bez with Lpp-GFP (M1)
831 and Lpp-GFP with Bez (M2). B) Fatty acid profile of the Lpp fraction as determined by mass
832 spectrometry. Heat maps show single measurements representing the percentage of species with
833 the indicated chain length. Bar charts show the same data. DG with a combined chain length of 28
834 carbons (14 carbons average chain length) are predominant in wildtype Lpp, but shifted towards
835 longer chains in Bez mutants. n = 3. Asterisks represent *** $p > 0.001$, ** $p > 0.01$, * $p > 0.05$, ns: not
836 significant.